Oxygen Binding by Single Crystals of Hemoglobin†

Claudio Rivetti,‡ Andrea Mozzarelli,*,‡ Gian Luigi Rossi,‡ Eric R. Henry,§ and William A. Eaton*,§

Institute of Biochemical Sciences, University of Parma, 43100 Parma, Italy, and Laboratory of Chemical Physics, Building 2, National Institute of Diabetes and Digestive and Kidney Diseases, National Institutes of Health, Bethesda, Maryland 20892

Received September 21, 1992; Revised Manuscript Received November 13, 1992

ABSTRACT: Reversible oxygen binding curves for single crystals of hemoglobin in the T quaternary structure have been measured using microspectrophotometry. Saturations were determined from complete visible spectra measured with light linearly polarized parallel to the *a* and *c* crystal axes. Striking differences were observed between the binding properties of hemoglobin in the crystal and those of hemoglobin in solution. Oxygen binding to the crystal is effectively noncooperative, the Bohr effect is absent, and there is no effect of chloride ion. Also, the oxygen affinity is lower than that of the T quaternary structure in solution. The absence of the Bohr effect supports Perutz's hypothesis on the key role of the salt bridges, which are known from X-ray crystallography to remain intact upon oxygenation. The low affinity and absence of the Bohr effect can be explained by a generalization of the MWC–PSK model (Monod, Wyman, & Changeux, 1965; Perutz, 1970; Szabo & Karplus, 1972) in which both high- and low-affinity tertiary conformations, with broken and unbroken salt bridges, respectively, are populated in the T quaternary structure. Because the α and β hemes make different projections onto the two crystal axes, separate binding curves for the α and β subunits could be calculated from the two measured binding curves. The approximately 5-fold difference between the oxygen affinities of the α and β subunits is much smaller than that predicted from the crystallographic study of Dodson, Liddington, and co-workers, which suggested that oxygen binds only to the α hemes. This 5-fold difference is exactly compensated by a small amount of cooperativity to produce the crystal binding curve with a Hill n of 1.0. In terms of free energy, the cooperativity is only about 10% of that observed in solution. It therefore represents only a slight perturbation on the essential feature of an allosteric model that the binding curve for hemoglobin in the T quaternary structure be perfectly noncooperative. If the concentration of the crystallizing agent [poly(ethylene glycol)] and/or the fraction of oxidized hemes are not sufficiently high, oxygen binding is no longer reversible. Under these conditions the crystals crack and undergo a time-dependent increase in their saturation with oxygen. We tentatively assume that this change corresponds to the conversion of the low-affinity T quaternary structure to the high-affinity R quaternary structure, opening up the possibility of carrying out a detailed kinetic study of the quaternary conformational change in the crystal by monitoring the oxygen saturation.

Hemoglobin remains the paradigm for understanding the cooperative behavior of proteins. The reason is that a surprisingly simple model can explain the major features of a vast array of structural, spectroscopic, equilibrium, and kinetic data on its cooperative ligand binding and conformational changes. The model is a synthesis of the two-state allosteric model of Monod, Wyman, and Changeux (Monod et al., 1965; Shulman et al., 1975; Edelstein, 1975), the stereochemical mechanism of Perutz (Perutz, 1970; Perutz et al., 1987), and the statistical mechanical formulation of Perutz's mechanism by Szabo and Karplus (Szabo & Karplus, 1972; Lee et al., 1988). Figure 1 shows schematic diagrams of this MWC–PSK model. The novel features of the model, and also the most controversial, are the central role of the salt bridges and the existence of only two affinity states of the tetramer, each with noncooperative binding. In later work Perutz suggested that there is indirect evidence from studies on mutant hemoglobins for cooperative oxygen binding to the T quaternary structure (Perutz, 1976, 1989). Ackers and co-workers have also proposed that there is significant cooperativity within both the R and T quaternary structures. Their conclusion is based on an analysis of the dimer–tetramer equilibrium constants of model compounds for the intermediate ligation states (Daugherty et al., 1991; Ackers et al., 1992). Finally, Shulman et al. (1982) pointed out that the failure of the salt bridges to break upon binding of carbon monoxide in crystals of the T-state mutant hemoglobin Kansas (Anderson, 1975) argues against Perutz's proposal for the role of the salt bridges.

It appeared to us that much of the controversy arises from the fact that the structural studies have been carried out on crystals, while the functional studies have been carried out on solutions where the structures are unknown. This pointed to a critical need for functional studies on crystals, permitting a direct comparison with the results of X-ray crystallography. Such comparisons have been found to be useful in the study of structure–function relations in enzymes (Rossi & Bernhard, 1970; Mozzarelli et al., 1989; Rossi et al., 1992). Our interest in this problem was further sparked by the determination of the structure of a partially oxygenated hemoglobin in the T quaternary structure (Brzozowski et al., 1984a; Liddington et al., 1988). This X-ray crystallographic investigation was carried out on crystals grown from solutions of poly(ethylene glycol) (PEG).[1] Unlike crystals formed in concentrated salt solution, which crack and become disordered upon oxygenation

† This work was supported in part by a binational grant from the National Research Council of Italy and by the Target Project on Biotechnology and Bioinstrumentation of the National Research Council of Italy.

* Correspondence may be addressed to either author.

‡ University of Parma.

§ National Institutes of Health.

[1] Abbreviations: oxyHb, oxyhemoglobin; deoxyHb, deoxyhemoglobin; metHb, methemoglobin; PEG, poly(ethylene glycol); DPG, 2,3-diphosphoglycerate; IHP, inositol hexaphosphate.

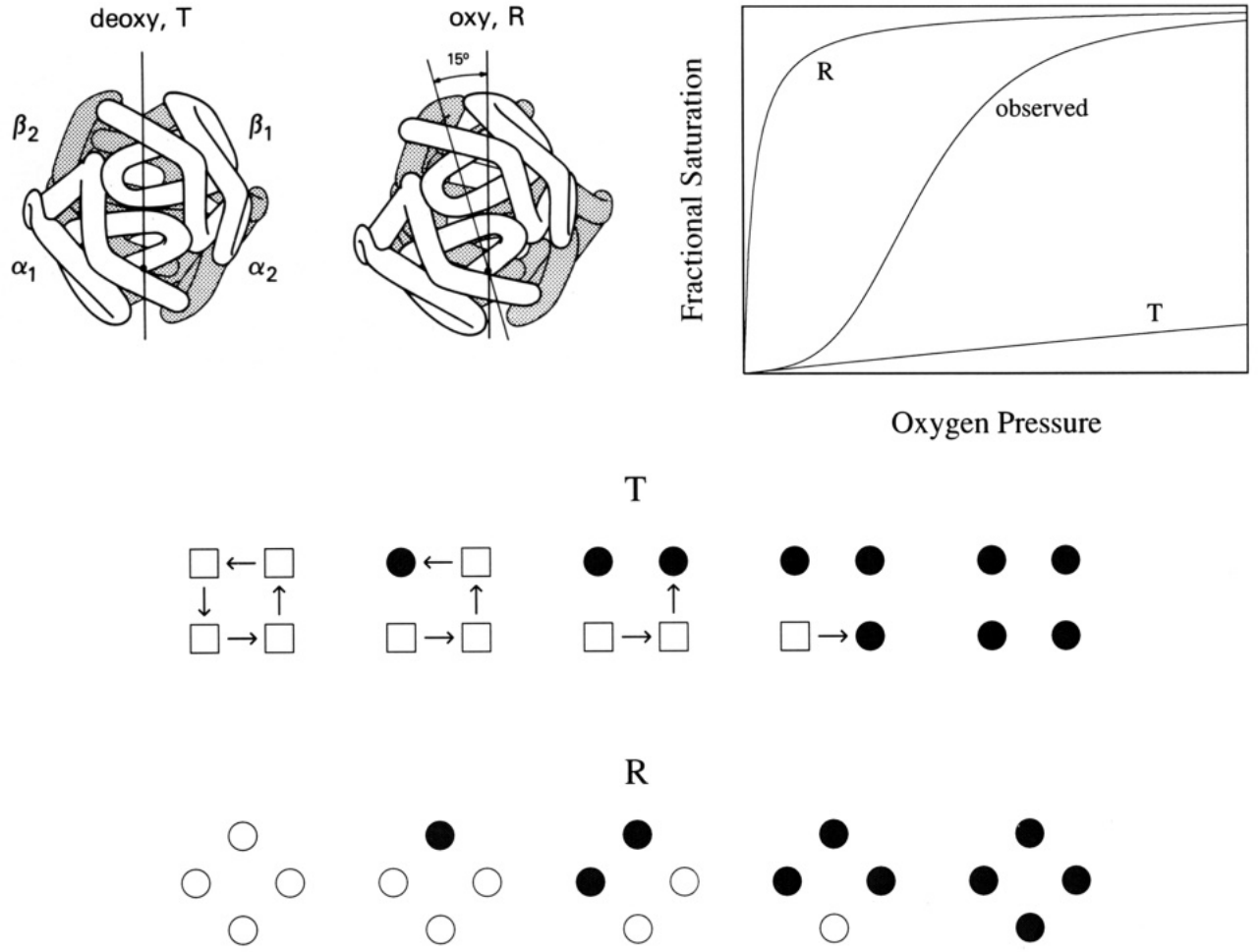

FIGURE 1: Schematic diagrams of MWC–PSK model for cooperative oxygen binding by hemoglobin. According to the model, hemoglobin exists in only two affinity states—a low-affinity T-state, corresponding to the quaternary structure of deoxyHb, and a high-affinity R-state, corresponding to the quaternary structure of oxyHb. Oxygen binding to either quaternary structure is noncooperative. That is, the intrinsic affinity of each heme for oxygen is independent of the number of oxygen molecules that are already bound. The observed cooperative binding curve is the result of a shift in the equilibrium between the two quaternary structures from the low-affinity T-state to the high-affinity R-state as successive molecules of oxygen bind. The quaternary conformational change consists of a rotation of the symmetrically related $\alpha\beta$ dimers by about 15° relative to each other and a translation of about 0.1 nm along the rotation axis. Six intersubunit salt bridges in the T quaternary structure that are not present in the R quaternary structure are key structural elements. These salt bridges may be thought of as "cross-links" between the $\alpha\beta$ dimers. They stabilize the T quaternary structure relative to R, act as the constraints that cause the low affinity of the T-state, and upon breaking release the protons that are responsible for the Bohr effect (the decrease in oxygen affinity with decreasing pH that facilitates unloading the oxygen in the acid-producing tissues). There are, in addition, two *intra*subunit salt bridges in the β subunits that release protons upon oxygen binding in either the R or T quaternary structures. In the absence of intersubunit salt bridges the R quaternary structure is more stable than T and the affinity is high. In the T quaternary structure, oxygen binding causes the movement of the iron toward the heme plane and an associated tertiary conformational change of the protein which breaks the salt bridge(s) originating from the carboxy terminus of that subunit. A subtle, but important, aspect of the mechanism is that breakage of the salt bridge in the T-state upon ligation of the subunit from which the salt bridge originates does not affect the affinity of the adjacent unliganded subunit to which the salt bridge was attached. Otherwise the T-state would not bind oxygen noncooperatively (Hess & Szabo, 1979). The residues on the adjacent subunits that form the salt bridges with the carboxy termini [Val 1 (NA1), Lys 40 (C5), and Asp 126 (H9) of the α subunits] are not directly coupled to the heme complex, so it is not unreasonable to assume that breakage of the salt bridges does not affect the affinity of the adjacent subunit. After two or three oxygen molecules have bound with the low, T-state association constant, the loss of the salt bridges originating from the liganded subunits sufficiently destabilizes the T quaternary structure that the R quaternary structure becomes more favorable. Binding to the remaining deoxyheme(s) then proceeds with the high, R-state association constant. Four of the eight salt bridges contain ionizable groups, and their breakage produces a change in pK of the participating residues that leads to a net release of protons. Release of protons upon binding to the T quaternary structure is called the "tertiary Bohr effect", while release of protons upon the change of quaternary structure is called the "quaternary Bohr effect". (Top Left) Quaternary conformational change [adapted from Dickerson and Geis (1983) and Baldwin and Chothia (1979)]. (Top Right) Observed binding curve and corresponding hyperbolic (noncooperative) binding curves for the R- and T-states. Binding begins along the T-state binding curve. As successive molecules of oxygen bind, the equilibrium between the two quaternary structures is shifted toward R, and subsequent binding occurs along the R-state binding curve. (Bottom) Simplified diagram of relation of salt bridges to tertiary and quaternary structure (adapted from Hess and Szabo (1979)]. Unliganded subunits are designated by open symbols and liganded subunits by filled symbols. These diagrams show the hypothetical situation in which each subunit is connected to two neighboring subunits by single salt bridges. Binding a ligand in the T quaternary structure causes a change in tertiary conformation from a square to a circle which breaks the salt bridge originating from that subunit, while the change from the T to R quaternary structure at any ligation state breaks all four salt bridges. The relation of the equilibrium constant for forming a salt bridge, S, and the quaternary equilibrium constant for the completely unliganded molecule in the absence of salt bridges, Q_0, to the MWC parameters K_T, K_R, and L is simply $K_T = K_R/S$ and $L = Q_0S^4$ (Hess & Szabo, 1979). These relations show that ligand binding to the T-state occurs with an association constant that is simply the R-state association constant reduced by a factor which is proportional to the strength of the salt bridge that is broken.

(Haurowitz, 1938; Perutz, 1953; Perutz et al., 1964), presumably due to a change from the T to R quaternary structure, the PEG crystals remained intact in air. As in all other liganded molecules in the T quaternary structure (Arnone et

al., 1986; Perutz et al., 1987; Luisi & Shibayama, 1989; Luisi et al., 1990; Abraham et al., 1992) the salt bridges were found to be intact (albeit at a single pH of 7.0 ± 0.2). The surprising result was that oxygen molecules were observed bound only to the α hemes, with no binding to the β hemes.

These findings suggested that it would be possible to measure oxygen binding curves on hemoglobin in the T quaternary structure, where both the tertiary and quaternary structures could be unambiguously defined by X-ray crystallography. An additional advantage of working with these particular crystals is that it is possible to make measurements under conditions close to those in solution, since PEG lowers the solubility of hemoglobin through its excluded volume effect and does not penetrate the crystal (McPherson, 1976, 1985, 1990; Ray et al., 1991). In this paper we present our initial results on the oxygen binding properties of single crystals from polarized optical absorption measurements using a microspectrophotometer. The study focuses on the questions of the degree of cooperativity within the T quaternary structure, the inequivalence in oxygen binding to the α and β hemes, and the effect of pH on the crystal binding curves. According to the MWC–PSK model, the maintenance of the T quaternary structure with intact salt bridges predicts a noncooperative crystal binding curve that is pH-independent. Furthermore, the conclusion from the X-ray studies that oxygen binds exclusively to the α hemes in air predicts that the crystal binding curve is distinctly biphasic. The present experiments directly test these predictions. A preliminary report of part of this work has appeared elsewhere (Mozzarelli et al., 1991).

MATERIALS AND METHODS

Preparation of Crystals for Microspectrophotometry. Human hemoglobin from a nonsmoker was purified using DEAE-Sephadex (A-50) chromatography according to procedures previously described (Dozy et al., 1968; Williams & Tsay, 1973). After concentration to about 0.1 g/mL and dialysis against 10 mM potassium phosphate buffer (pH 7.2, containing 1 mM EDTA), the solution was deoxygenated with nitrogen. Solutions for crystallization were prepared similarly to that previously described (Ward et al., 1975) by mixing the deoxyHb solution with various volumes of nitrogen-saturated, stock solution of poly(ethylene glycol) (PEG, 8000 MW, from Sigma), purified as described previously (Ray & Puvathingal, 1985). The stock PEG solution was composed of 50 g of PEG dissolved in 100 mL of 14 mM potassium phosphate buffer (1.4 mM EDTA) to give a final concentration of 36% (w/v) PEG and 10 mM potassium phosphate (1.0 mM EDTA), with the final pH adjusted to 7.2 with an identical PEG solution containing phosphoric acid instead of potassium phosphate. Solid sodium dithionite was added to give a final concentration of 30 mM. Crystals of sufficient size for microspectrophotometry usually appeared (together with much larger crystals) within 2–3 days at 4 °C in hemoglobin/PEG volume ratios of 8.3/1.7 to 8.7/1.3. The crystals were rectangular plates, an ideal morphology for microspectrophotometry. Lower hemoglobin/PEG ratios resulted in precipitation of the hemoglobin and crystals that were too small, while higher ratios did not yield crystals.

Crystals were transferred anaerobically at 4 °C to a PEG solution of concentration 36% or greater in two steps, first to a 20% PEG solution containing 30 mM sodium dithionite and then to a more concentrated dithionite-free PEG solution. The dithionite and precipitated hemoglobin were then removed by sedimenting and resuspending the crystals in the final deoxygenated PEG solution at least 6 times. To minimize metHb formation the PEG solution used for washing the crystals also contained 30–90 μg/mL catalase (Sigma).

Measurement of Polarized Absorption Spectra and Oxygen Pressures. For spectral measurements a single crystal with about 10 μL of its suspending medium was placed on a glass cover slip at 4 °C in air or under nitrogen and covered with a silicon copolymer membrane (General Electric MEM 213) (Gill, 1981). This membrane is gas-permeable and does not depolarize linearly-polarized light. The cover slip/membrane assembly was then sealed into a Dvorak–Stotler flow cell (Dvorak & Stotler, 1971).

Single-crystal polarized absorption spectra at each oxygen pressure were measured with a Zeiss MPM03 microspectrophotometer equipped with 10× ultrafluar-pol objectives and Glan–Thompson-type polarizing prisms to produce linearly-polarized light. These objectives are relatively strain-free and do not significantly depolarize the light (ratio of transmitted light between parallel and crossed polarizers of >8000:1). The crystal was thermostated by contact of the flow cell with the water-thermostated microscope stage and isolation of the supra- and substage objectives with Armaflex (Armstrong). Temperatures were measured with a thermistor in contact with the microscope stage. The measured temperature was corrected for thermal gradients (<4 °C) in a separate calibration experiment in which a second thermistor was placed in the position of the crystal in the flow cell. The transmitted light through the crystal, doubly masked with the image of a field diaphragm and a circular mask at the image plane of the suprastage objective, was measured with the light polarized parallel to the two orthogonal extinction directions of the crystal. The extinction directions were always parallel to the crystal edges. The region immediately adjacent to the crystal was used to measure the incident intensity. Optical densities were recorded at 1-nm intervals on a HP9816 calculator (Hewlett-Packard).

X-ray precession photography showed that the crystals used in this study belong to the same space group ($P2_12_12$), with the same unit cell dimensions as reported previously (Liddington et al., 1988). The crystals are flattened on the (010) face with the a and c axes of the orthorhombic unit cell parallel to the crystal edges. The more strongly absorbing direction of the crystal was, with rare exception, parallel to the shorter axis of the crystal, assigning it to the a crystal axis on the basis of the optical properties calculated from the heme orientations (Table I).

The oxygen pressure in equilibrium with the crystal suspension was varied in discrete steps by flowing mixtures of oxygen and helium prepared with mass flow controllers (Environics, Series 200). All gases were at least 99.95% pure and were transferred through 316 stainless steel tubing (Alltech-Europe) (Mills et al., 1976). Humidification was performed by bubbling the gas mixture through either water or the PEG solution used for suspending the crystals. Oxygen pressures were measured in the outflow of the cell containing the crystal suspension using a Clark polarographic electrode, thermostated at either 15 or 20 °C, and oxygen meter (Oxyan 2, Advanced Products) (Rossi-Bernardi et al., 1977). The oxygen electrode was calibrated at the beginning and middle of each experiment with two humidified oxygen mixtures (4.88% and 21.23% oxygen/balanced helium) and at the end of the experiment with humidified 99.95% oxygen. The oxygen pressures were calculated from the composition of the standard gases and the measured barometric pressure and were corrected for the partial pressure of water at each temperature obtained

Table I: Projection of Heme Planes and Polarization Ratios in Crystals of Hemoglobin with the T Quaternary Structure

subunit	$\sin^2 z_i a^a$	$\sin^2 z_i b^a$	$\sin^2 z_i c^a$	$P(x,y)_{calc}{}^b$	$P(x,y)_{obs}$ Soret[c]	$P(x,y)_{obs}$ visible[d]
			Deoxyhemoglobin[e]			
α_1	0.754	0.527	0.718			
α_2	0.787	0.815	0.398	1.69	1.69 ± 0.01	1.77
β_1	0.884	0.856	0.260			
β_2	0.795	0.675	0.530			
			"Semioxyhemoglobin"[f]			
α_1	0.739	0.535	0.726			
α_2	0.779	0.824	0.397	1.63		
β_1	0.875	0.860	0.265			
β_2	0.784	0.651	0.565			
			"Oxyhemoglobin"[g]			
α_1	0.739	0.535	0.726			
α_2	0.779	0.824	0.397	1.49	1.47 ± 0.01	1.41
β_1	0.825	0.848	0.327			
β_2	0.748	0.624	0.628			
			Methemoglobin[h]			
α_1	0.731	0.556	0.713			
α_2	0.774	0.819	0.407	1.60	1.56 ± 0.01	1.61
β_1	0.855	0.873	0.271			
β_2	0.769	0.670	0.561			

Geometric Factors of Eq 9[i]

$n_{deoxy,a}$	0.479	$n_{oxy,a}$	0.491	$n_{met,a}$	0.481
$n_{deoxy,c}$	0.586	$n_{oxy,c}$	0.541	$n_{met,c}$	0.574

[a] $z_i a$, $z_i b$, and $z_i c$ are the angles between the normal to the plane of the heme chromophore (taken as the z molecular axis) and the crystal axes a, b, and c. The plane of the heme chromophore was calculated as the least-squares best plane through the 24 porphin skeletal atoms. [b] Calculated from eq 6. [c] Calculated from the ratio of the areas under the Soret bands from $1/e$ to $1/e$ of the peak height. [d] Calculated from the ratio of the areas in the spectral regions 525–580 and 630–650 nm. [e] Calculated from the $P2_12_12$ structure of Liddington (unpublished results). [f] Calculated from the structure of Liddington et al. (1988). [g] The squared sines for the α hemes were calculated from the orientation of the α oxyhemes of semioxyhemoglobin (Liddington et al., 1988). The squared sines for the β hemes were calculated using the structure of the nickel–iron hybrid hemoglobin, $\alpha(Ni)_2\beta(FeCO)_2$, in which the iron atoms of the α hemes were replaced by nickel(II) atoms and the β hemes are liganded with carbon monoxide (Luisi et al., 1990). This molecule crystallizes from PEG in a different space group ($P2_1$) than "semioxyhemoglobin". The β subunits of $\alpha(Ni)_2\beta(FeCO)_2$ were oriented relative to the unit cell axes of the PEG deoxyHb structure by a least-squares superposition of all of the backbone atoms onto the β subunits of deoxy Hb. [h] Calculated from the $P2_12_12$ structure of Liddington (unpublished results). [i] These are the geometric factors as defined in eq 9 and calculated from the squares sines listed above. They represent the fractional projection, and therefore the fractional contribution, of the α hemes to the absorption measured along the a and c crystal axes in regions of the spectrum where the heme behaves like a circular absorber.

from standard tables. The deviation from linearity and drift of the electrode were less than 1% and 0.3%/h, respectively.

In a typical experiment to determine an oxygen binding curve, polarized spectra between 450 and 700 nm were recorded in both polarizations at 7–12 different oxygen pressures between 0 and 1 atm of oxygen. The crystal dimensions were usually about 150 μm by 200 μm, with a thickness of about 20 μm (calculated from the solution extinction coefficients using eq 5). Following a step change in oxygen pressure, the time required for equilibration of the system, as determined by stable values for both the optical density and electrode current, was 30–45 min at a gas flow rate of 50 mL/min. Recording of spectra required an additional 20 min, so that the total time required for the experiment was at least 7 h.

Optical Theory. In this section we present the theory of polarized optical absorption measurements on single crystals that is essential for interpreting the experiments described in this work. Additional information on single-crystal spectroscopy of hemoglobin can be found elsewhere (Hofrichter & Eaton, 1976; Eaton & Hofrichter, 1981).

For solution studies of oxygen binding the Beer–Lambert law is

$$\mathrm{OD} = cl\sum_i f_i\epsilon_i \qquad (1)$$

where c is the total heme concentration, l is the path length, f_i is the fraction of species i (oxyheme, deoxyheme, or metheme), and ϵ_i is the molar extinction coefficient at the wavelength of the measurement. In principle there should be additional terms to account for differences in extinction coefficients and oxygen affinities of α and β hemes and the dependence of the extinction coefficients on the ligation state of the tetramer. These effects are, however, small and have only recently been investigated (Ownby & Gill, 1990).

For binding studies of single crystals the analogous equation is

$$\mathrm{OD}_\mu = cl\sum_i f_i\epsilon_{i\mu} \qquad (\mu = a, b, c) \qquad (2)$$

where OD_μ is the optical density measured for linearly polarized light with its electric vector parallel to the μ crystal direction, c is the concentration of hemes in the crystal, which can be calculated from the number of molecules in the unit cell and its dimensions, l is the crystal thickness, f_i is the fraction of species i, and $\epsilon_{i\mu}$ is the molar extinction coefficient of species i for light polarized parallel to the μ crystal direction. Equation 2 indicates that the extinction coefficients are different for different crystal directions. It also implies that, unlike solution spectra, crystal spectra must be measured with linearly-polarized light. The electric vector of the light must be parallel to a principal optical direction in the crystal to ensure that it remains linearly polarized as it propagates through the crystal. Lambert's law of exponential attenuation of the light intensity does not hold if this condition is not satisfied. The symmetry of the unit cell of the crystals employed in this study is orthorhombic (space group $P2_12_12$) (Brozozowski et al., 1984; Liddington et al., 1988). For orthorhombic crystals, the a, b, and c crystal axes are principal optical directions, and all of the spectra in this study have been measured with the light incident on the (010) (ac) crystal face with light polarized parallel to either the a or c crystal axes.

Crystal extinction coefficients are different for each axis because the projections of the hemes are different. Figure 2 shows the projection of the four hemes of the hemoglobin molecule onto the ac crystal face of deoxyHb. Upon expressing the crystal extinction coefficients, $\epsilon_{i\mu}$, in terms of the heme molecular extinction coefficients, ϵ_{ijk}, and angles, $k_{ij}\mu$, between the k_{ij} heme axis and the μ crystal axis, eq 1 becomes (Hofrichter & Eaton, 1976; Eaton & Hofrichter, 1981)

$$\mathrm{OD}_\mu = \frac{cl}{4}\sum_i\sum_{j=1}^{4}\sum_{k=x,y,z} f_{ij}\epsilon_{ijk}\cos^2 k_{ij}\mu \qquad (\mu = a, b, c) \qquad (3)$$

The index i denotes the heme species (oxyheme, deoxyheme, metheme), the index j denotes the four hemes of the hemoglobin molecule (α_1, α_2, β_1, β_2), and the index k denotes the heme molecular axis (x, y, z).

Equation 3 indicates that there are two types of information in polarized crystal spectra that are not present in solution spectra. First, the α and β hemes make different contributions to the absorption along the a and c crystal axes (Figure 2), so that it is possible in principle to determine their relative oxygen affinities. Second, changes in heme orientation, for

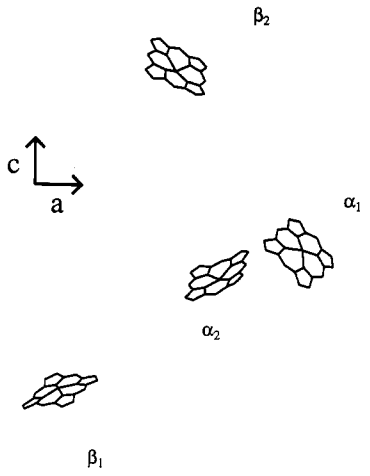

FIGURE 2: Projection of the four hemes of the asymmetric unit of the deoxyHb crystal onto the *ac* (010) crystal face. For all four hemes there is a larger projection of the 24-atom porphin ring onto the *a* crystal axis than onto the *c* crystal axis. For the *a* axis the projections of the α and β hemes are roughly equal, while for the *c* axis there is a larger projection of the α hemes (see Table I).

example those accompanying conformational changes associated with oxygen binding, produce changes in the crystal extinction coefficients by changing the $\cos^2 k_{ij}\mu$ terms (Makinen & Eaton, 1974; Eaton & Hofrichter, 1981). An analysis of these effects is more straightforward for regions of the optical spectrum where the high effective symmetry of the heme chromophore results in simplifications of the relations between the molecular extinction coefficients.

For a heme chromophore that possesses a perfect 4-fold rotation axis, transitions can either be polarized parallel to the normal to the heme plane, called *z*-polarized transitions, or perpendicular to the heme normal, called *x,y*-polarized transitions. For *x,y*-polarized transitions, the absorption is maximal and equal for all directions of the electric vector of linearly polarized light perpendicular to the heme normal and is zero parallel to the heme normal; i.e., $\epsilon_z = 0$ and $\epsilon_x = \epsilon_y = (^3/_2)\bar{\epsilon}$, where $\bar{\epsilon}$ is the solution (isotropic) extinction coefficient. A heme with these relations among the molecular extinction coefficients is said to behave like a circular absorber of linearly-polarized light. For *z*-polarized transitions the absorption is maximal for the electric vector parallel to the heme normal and is zero when it is perpendicular; i.e., $\epsilon_x = \epsilon_y = 0$ and $\epsilon_z = 3\bar{\epsilon}$. The solution extinction coefficient, $\bar{\epsilon}$, is related to the crystal extinction coefficients (for any polarization or composition) measured along the three orthogonal crystal axes by

$$\bar{\epsilon} = \frac{1}{3}\sum_{\mu=a,b,c} \epsilon_\mu \qquad (4)$$

Most of the absorption intensity between 450 and 700 nm, the spectral region used in this study, is *x,y*-polarized. The optical density for an *x,y*-polarized transition of a single species is, from eq 3

$$\mathrm{OD}_\mu(x,y) = \frac{3}{8}cl\bar{\epsilon}\sum_{j=1}^{4} \sin^2 z_j\mu \qquad (5)$$

where we have assumed that the spectra for all four hemes of the tetramer (the asymmetric unit of the unit cell) are identical. The polarization ratio, defined as the ratio of optical densities for orthogonal crystal directions, is a very useful quantity because it is independent of the extinction coefficients and only depends on the heme orientations. For the *ac* crystal face it is given by

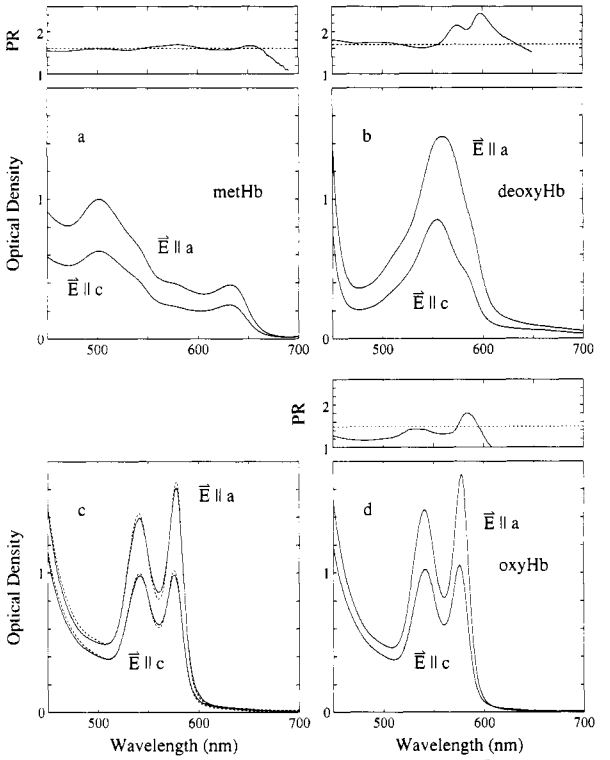

FIGURE 3: Reference crystal and polarization ratio spectra. These are the spectra of the pure species measured with the electric vector of the linearly-polarized light parallel to either the *a* (upper curve) or *c* (lower curve) crystal axes. The polarization ratio at each wavelength, defined as the ratio of the *a*-axis to the *c*-axis optical densities, is plotted above the spectra. The dashed line is the value for an *x,y*-polarized transition calculated from the heme orientations determined by X-ray crystallography (eq 6). The spectra have been scaled for differences in crystal thickness, so that the relative crystal optical densities are the same as the relative crystal extinction coefficients. (a) MetHb spectra at pH 7.2, 20 °C. (b) DeoxyHb spectra at 20 °C. (c) Observed spectra at 7 °C at 1 atm of oxygen (continuous curves) and the spectra extrapolated to infinite oxygen pressure as described in the text (dashed curves). (d) OxyHb spectra. These are the spectra obtained after subtracting the contribution of metheme spectra from the extrapolated spectra (dashed curves in panel c) as described in the text and rescaling for the apparent fraction of methemes.

$$P(x,y) \equiv \frac{\mathrm{OD}_a(x,y)}{\mathrm{OD}_c(x,y)} = \frac{\sum_{j=1}^{4} \sin^2 z_j a}{\sum_{j=1}^{4} \sin^2 z_j c} \qquad (6)$$

The values for the heme orientation terms, $\sin^2 z_j a$ and $\sin^2 z_j c$, are obtained from the X-ray coordinates and are given in Table I.

For multiple species, eq 5 becomes

$$\mathrm{OD}_\mu(x,y) = \frac{3}{8}cl\sum_i \sum_{j=1}^{4} f_{ij}\bar{\epsilon}_i \sin^2 z_{ij}\mu \qquad (7)$$

If the fraction of each species is the same for the two α hemes and for the two β hemes, i.e., $f_{i,\alpha 1} = f_{i,\alpha 2} \equiv f_{i\alpha}$ and $f_{i,\beta 1} = f_{i,\beta 2} \equiv f_{i\beta}$, then substitution for the isotropic extinction coefficients in eq 7 from eq 5 yields

$$\mathrm{OD}_\mu(x,y) = s\sum_i \mathrm{OD}_{i\mu}[f_{i\alpha}n_{i\mu} + f_{i\beta}(1 - n_{i\mu})] \qquad (8)$$

where $\mathrm{OD}_{i\mu}$ is the optical density of the pure species *i*, *s* is a

scale factor to correct for the difference between the thickness of the crystal being measured and that of the crystal used in obtaining the reference spectra ($OD_{i\mu}$), and $n_{i\mu}$ are geometric factors, which are the fractional projection of the α hemes onto the crystal axes and are given by (Table I)

$$n_{i\mu} = \frac{\sum_{j=1}^{2} \sin^2 z_{i,\alpha j\mu}}{\sum_{j=1}^{2} (\sin^2 z_{i,\alpha j\mu} + \sin^2 z_{i,\beta j\mu})} \quad (9)$$

Equation 8 is the working equation for obtaining the composition of the crystal in terms of the fraction of oxy, deoxy, and met species. This composition is obtained by varying the values of the six composition parameters ($f_{i\alpha}$ and $f_{i\beta}$, i = oxy, deoxy, and met, with the constraint that $0 < f_{ij} < 1$) in a simultaneous least-squares fit of the measured optical densities polarized parallel to both the a and c axes [$OD_\mu(x,y)$] using oxyheme, deoxyheme, and metheme reference spectra ($OD_{i\mu}$). In carrying out this fit, wavelength regions were selected where the polarization is close to x,y for all three species. The fractional saturation values of the reduced hemes, y_α and y_β, are defined as

$$y_\alpha \equiv \frac{f_{\text{oxy},\alpha}}{f_{\text{oxy},\alpha} + f_{\text{deoxy},\alpha}} \qquad y_\beta \equiv \frac{f_{\text{oxy},\beta}}{f_{\text{oxy},\beta} + f_{\text{deoxy},\beta}} \quad (10)$$

In the case where there is no oxidation or equal oxidation of the methemes ($f_{\text{met},\alpha} = f_{\text{met},\beta}$), it is possible to obtain analytical relations between the apparent saturations, y_a and y_c, and the saturations of the α and β hemes, y_α and y_β. The relation between the saturations of the α and β hemes, y_α and y_β, and the apparent saturations y_a and y_c is given by

$$y_a = \frac{y_\alpha n_{\text{oxy},a} + y_\beta(1 - n_{\text{oxy},a})}{y_\alpha n_{\text{oxy},a} + y_\beta(1 - n_{\text{oxy},a}) + (1 - y_\alpha)n_{\text{deoxy},a} + (1 - y_\beta)(1 - n_{\text{deoxy},a})}$$

$$y_c = \frac{y_\alpha n_{\text{oxy},c} + y_\beta(1 - n_{\text{oxy},c})}{y_\alpha n_{\text{oxy},c} + y_\beta(1 - n_{\text{oxy},c}) + (1 - y_\alpha)n_{\text{deoxy},c} + (1 - y_\beta)(1 - n_{\text{deoxy},c})} \quad (11)$$

Rearrangement of eq 11 results in

$$y_\alpha = \frac{y_c(1 - \zeta_a) - y_a(1 - \zeta_c)}{\zeta_c - \zeta_a}$$

$$y_\beta = \frac{y_a\zeta_c - y_c\zeta_a}{\zeta_c - \zeta_a} \quad (12)$$

where we have defined

$$\zeta_a \equiv n_{\text{oxy},a} - y_a(n_{\text{oxy},a} - n_{\text{deoxy},a})$$

$$\zeta_c \equiv n_{\text{oxy},c} - y_c(n_{\text{oxy},c} - n_{\text{deoxy},c}) \quad (13)$$

If the binding curve for each subunit is noncooperative (Hill $n = 1$)

$$y_\alpha = \frac{p}{p + p50_\alpha} \qquad y_\beta = \frac{p}{p + p50_\beta} \quad (14)$$

Substituting eq 14 into eq 11 and rearranging results in a relation between the apparent $p50$'s, $p50_a$ and $p50_c$, and the $p50$'s for the individual subunits, $p50_\alpha$ and $p50_\beta$, for the case of equal or no oxidation of the α and β hemes

$$p50_{\alpha,\beta} = \frac{1}{2}\frac{p50_c^2 - p50_a^2}{p50_a h_a - p50_c h_c}\left\{\mp 1 + \left[1 + \frac{4p50_a p50_c[p50_a p50_c(h_a^2 + h_c^2) - (p50_c^2 + p50_a^2)h_a h_c]}{(p50_c^2 - p50_a^2)^2}\right]^{1/2}\right\} \quad (15)$$

where to simplify the notation we have defined

$$h_a = n_{\text{oxy},a} + n_{\text{deoxy},a} - 1 \qquad h_c = n_{\text{oxy},c} + n_{\text{deoxy},c} - 1 \quad (16)$$

The minus sign in the $\mp$ applies for $p50_\alpha$ and the plus sign for $p50_\beta$.

For purposes of reporting primary data, it is useful to define apparent composition parameters, $g_{i\mu}$, that are independent of the geometric factors

$$OD_\mu = s\sum_i g_{i\mu} OD_{i\mu} \quad (17)$$

and apparent saturations as

$$y_a = \frac{g_{\text{oxy},a}}{g_{\text{oxy},a} + g_{\text{deoxy},a}} \qquad y_c = \frac{g_{\text{oxy},c}}{g_{\text{oxy},c} + g_{\text{deoxy},c}} \quad (18)$$

The three composition parameters for each crystal axis are obtained from a least-squares fit of the reference spectra to the measured spectra using the measured optical densities at all 251 wavelengths in the range 450–700 nm.

Determination of Reference Spectra. The long time required for measurement of complete binding curves resulted in the oxidation of a substantial fraction of the hemes. This, together with the low affinity of the crystal for oxygen, made it impossible to accurately determine the fractional saturation of the hemes from optical density measurements at single wavelengths as is usually done in solution experiments. We therefore determined the composition of the crystal from measurements of complete spectra in the visible region (450–700 nm).

As indicated by eqs 8 and 17, determination of the fraction of oxyhemes, deoxyhemes, and methemes requires knowledge of the spectra of the pure species, which we call reference spectra. The determination of reference spectra for metHb and deoxyHb was straightforward (Figure 3a,b). The only problem was to obtain accurate *relative* crystal extinction coefficients. Absolute crystal extinction coefficients are not known since the crystal thicknesses could not be accurately determined. Relative crystal extinction coefficients were obtained by measuring the deoxyHb and metHb spectra on the identical crystal according to the following procedure. First, the crystals were oxidized with 5 mM potassium ferricyanide in the 36% PEG solution. After being washed with the 36% PEG solution to remove the oxidizing agent and measuring the metHb spectrum, the crystals were washed with a deoxygenated 36% PEG solution and then with a deoxygenated 36% PEG solution containing 30 mM sodium dithionite to reduce the crystal for measurement of the deoxyHb spectrum. Spectra in both the met and deoxy forms were measured on several crystals. The unit cell dimensions of the deoxyHb and metHb crystals are identical, indicating that there is no change in the concentration of hemes or optical path length accompanying the change in oxidation state

(Liddington et al., 1988). Because the spectra of metHb are strongly pH dependent due to the ionization of the iron-bound water molecule, spectra of metHb at pH's other than 7.2 were determined in separate experiments by exchanging the PEG solution bathing the crystal in situ. These experiments were carried out both in the phosphate buffer and in the bis-Tris and Tris buffers at 0.2 M chloride ion to give a constant ionic strength.

The determination of reference spectra of oxyHb was made difficult by oxidation and by incomplete saturation of the reduced hemes even at 1 atm of oxygen. To obtain spectra with no contribution of deoxyHb, experiments were performed at 5–8 °C [58% (w/v) PEG and 5 mM potassium phosphate buffer, pH 7.2], where the oxygen affinity is relatively high ($p50 \approx 70$ Torr). Data were extrapolated to infinite oxygen pressure by straight-line fits to plots of the reciprocal of the ΔOD at each of the 251 wavelengths from 450 to 700 nm versus the reciprocal of the oxygen pressure. The difference optical density, ΔOD, was calculated as the optical density at each pressure minus the optical density at zero pressure. Only the highest oxygen pressures (300–750 Torr) were used in this double-reciprocal plot. The procedure is approximate for two reasons. First, the dependence on oxidation and oxygenation is different but is assumed to have the same pressure dependence in the extrapolation. Second, the double-reciprocal plot biases the extrapolated values to be those that would be obtained for a perfectly hyperbolic, i.e., noncooperative, binding curve. These should, however, only have small effects on the final binding curve, since the extrapolation was made over a range of pressures in which the change in the saturation with oxygen was less than about 10% and the change in metHb was less than about 2%. To remove the contribution of metHb to the extrapolated spectra, various fractions of the metHb reference spectra were subtracted until the metHb band at 630 nm was no longer discernible. Figure 3c shows the observed spectra from one of these experiments at 1 atm of oxygen and the extrapolated spectra, and Figure 3d shows the spectra corrected for metHb, which was 4% with an uncertainty of less than 2%. The relative crystal extinction coefficients were based on the optical densities at 555 nm of the zero pressure spectra, corrected for the presence of metHb by fitting to a linear combination of deoxyHb and metHb reference spectra.

To obtain the apparent saturations for each crystal axis the observed spectra at each pressure were fit with a linear combination of the spectra in Figure 3, panels a, b, and d, plus an offset, thereby determining the fraction of deoxyhemes, oxyhemes, and oxidized hemes (eqs 17 and 18). The offset was used to account for small shifts in the baseline, which were less than 2% of the maximum optical density, resulting from changes in the incident light intensity between measurements on the crystal and the area adjacent to the crystal. Intensity changes were caused by slight adjustments in the optics accompanying changes in the position of the flow cell or rotation of the polarizer.

Determination of Geometric Factors. In the section on Optical Theory we showed how to exploit the small difference in the projections of the α and β hemes onto the *a* and *c* crystal axes to obtain the individual saturations for the α and β subunits (eqs 8–10, 12, and 13). To do so requires that the hemes behave like circular absorbers of linearly-polarized light in the wavelength region of the measurements, as well as knowledge of the heme orientations. Hemes are most nearly perfectly circular absorbers of linearly-polarized light in the Soret region (Eaton & Hochstrasser, 1967, 1968; Makinen & Eaton, 1974; Hofrichter & Eaton, 1976; Eaton & Hofrichter, 1981). Figure 4 shows the spectra in the Soret region for oxyHb, deoxyHb, and metHb and the polarization ratios at each wavelength. The ratio of the Soret band areas is compared to the prediction from the heme orientations (eq 6) determined by X-ray crystallography in Table I.

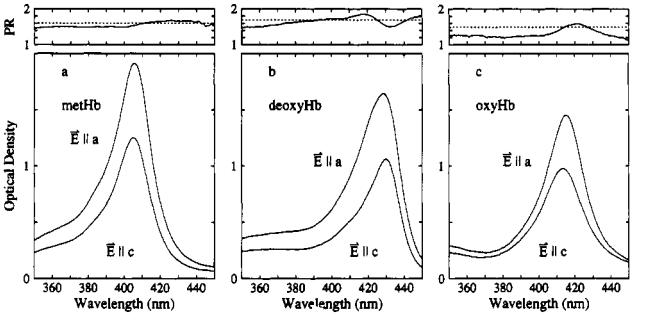

FIGURE 4: Polarized absorption and polarization ratio spectra in Soret region. The dashed line is the value for an *x,y*-polarized transition calculated from the heme orientations determined by X-ray crystallography (eq 6). (a) MetHb. The spectrum was measured after first fully oxidizing the crystal with potassium ferricyanide and then washing with 36% (w/v) PEG buffered with 10 mM potassium phosphate at pH 6.2. (b) DeoxyHb. The spectrum was obtained after reduction of the same crystal with sodium dithionite. (c) OxyHb. The dithionite was washed away, and the crystal was exposed to 1 atm of oxygen at 8 °C. The metHb spectrum was subtracted from the observed spectrum, using the fraction obtained from fits in the region 450–700 nm (eq 11). The fraction of methemes and deoxyhemes in the observed spectrum was determined by fitting the data in the region 450–700 nm (eq 17) and was subtracted using the spectra in panels a and b. The resulting spectrum was then rescaled to 100% oxyHb by dividing the optical densities by $(1 - g_{met,a} - g_{deoxy,a})$ or by $(1 - g_{met,c} - g_{deoxy,c})$.

For deoxyHb and metHb there is excellent agreement between the polarization ratios calculated from the heme orientation in the crystal and the observed values for the integrated Soret band areas. Since the X-ray study was not carried out on a fully saturated crystal, it is problematic as to how to predict the optical properties of fully oxygenated hemoglobin from the available heme atomic coordinates. In addition, as discussed later, there is a significant discrepancy in the occupancy of the ligand binding sites determined by the X-ray and optical studies. According to our data the electron density map should be complex, because there are contributions from three structures, subunits with deoxyhemes, subunits with oxygenated hemes, and subunits with oxidized hemes. The X-ray refinement was apparently carried out, however, assuming a single structure. In any event, in the structure of "semioxyhemoglobin" there is very little change in α heme orientation. This is also the case for carbon monoxide binding to the α hemes in the T quaternary structure of the iron–cobalt and iron–nickel hybrid molecules, $\alpha(FeCO)_2\beta(Co)_2$ and $\alpha(FeO_2)_2\beta(Ni)_2$, in which cobalt(II) or nickel(II) has been substituted for iron in the β hemes (cobalt porphyrins do not bind carbon monoxide and nickel porphyrins do not bind oxygen) (Luisi & Shibayama, 1989). It is therefore reasonable to assume that in our fully oxygenated crystal the α heme orientation is not very different from that in deoxyHb.

The situation with the β hemes is less clear. If we use the coordinates from "semioxyhemoglobin" for both α and β hemes, the calculated polarization ratio is significantly higher than the observed value for the fully oxygenated crystal. If, however, we use the α heme orientation from "semioxyhemoglobin" [or from either of the other two α-liganded structures, $\alpha(FeCO)_2\beta(Co)_2$ or $\alpha(FeCO)_2\beta(Ni)_2$ (Luisi & Shibayama, 1989)] and the β heme orientation from the T-state

structure of Luisi et al. (1990) of the iron–nickel(II) hybrid molecule liganded with carbon monoxide, $\alpha(Ni)_2\beta(FeCO)_2$, the agreement is much better. We have therefore used these orientations in calculating the projections of the heme plane in Table I.

In order to utilize the spectra in the visible region for determining the α and β heme saturations, we must use wavelength regions of the spectra in which the heme behaves as a circular absorber, and also a region which has large spectral differences among the three species. In oxyHb, there is a significant contribution from z-polarized transitions below about 525 nm (Eaton & Hofrichter, 1981; Makinen & Churg, 1983) (which could be included in a more detailed theory), while in deoxyHb above 580 nm the absorption is no longer circular, presumably due to unequal x- and y-polarized intensity in the Q_0 band (Eaton & Hofrichter, 1981). MetHb poses no problem because it exhibits circular absorption throughout the entire visible region. In order to have a sensitive measure of the fraction of methemes, wavelengths near the 630-nm metheme peak were included that also have a polarization ratio for deoxyHb close to the value for a circular absorber. We have therefore chosen the regions 525–580 and 630–650 nm. The polarization ratios for the integrated areas in these regions are also given in Table I and are in reasonably good agreement with the Soret band areas and polarization ratios predicted by X-ray crystallography.

RESULTS

As was observed in the X-ray crystallographic studies, crystals in their mother liquor, which contained 5–6% (w/v) PEG, dissolved upon exposure to air, and dissolution was prevented by increasing the PEG concentration to 36% (w/v) (Grabowski et al., 1978; Brzozowski et al., 1984b). This change in PEG concentration decreases the solubility of hemoglobin when equilibrated with air at 4 °C from greater than 10 mg/cm^3 to about 0.02 mg/cm^3. At the higher PEG concentration the crystals still, however, occasionally developed cracks upon oxygenation. Crystals that developed cracks invariably exhibited an increase in oxygen affinity. Our working hypothesis has been that in intact crystals the hemoglobin molecules remain in the T quaternary structure and that the cracking of crystals signals the conversion of the quaternary structure from T to R, as evidenced by the increase in oxygen affinity.

Two factors were found to be critical for stabilizing the crystals against cracking upon oxygenation. These are the fraction of hemes that have oxidized to the met form and the concentration of PEG. The results of experiments demonstrating the stabilizing effect of methemes and PEG are shown in Figure 5. In one experiment the oxygen pressure for a crystal containing 36% (w/v) PEG and 3% methemes was increased from 0 to 160 Torr. The increase in saturation was biphasic, with an initial relatively rapid increase in saturation, followed by a much slower increase. This crystal developed fine cracks. In contrast, increasing either the PEG concentration or metheme content resulted in crystals which showed both stable and reversible behavior and did not develop cracks upon oxygenation. In the experiments shown in Figure 5 the metheme content of a crystal in 36% PEG was 14%, while in another crystal the PEG concentration of a crystal with a very low metheme content (3%) was 54% (w/v). Upon increasing the oxygen pressure from 0 to 160 Torr these crystals developed no cracks, and a much lower and stable saturation of 70% was reached.

In most of the following experiments the highest possible PEG concentration was employed [62% (w/v)]. Measurements at several concentrations of PEG between 36% and 62% (w/v) at pH 7.2, with a metheme content between 1% and 8%, showed no effect on the oxygen saturation at a fixed oxygen pressure of 154 Torr (data not shown) (Amiconi et al., 1977; Haire et al., 1981). At a concentration of 62% (w/v) PEG, crystals always remained intact between pH's 6.0 and 8.4 at all oxygen pressures up to 1 atm and exhibited reversible oxygen binding curves. Perfect reversibility of the binding curve is demonstrated in an experiment on a crystal at 15 °C (Figures 6–9). Figure 6 shows the polarized absorption spectra from this experiment at eight oxygen pressures between 0 and 760 Torr. The upper set of spectra is for the electric vector of the linearly-polarized light parallel to the a crystal axis, while the lower set of spectra is for light polarized parallel to the c crystal axis. The observation of isosbestic points indicates

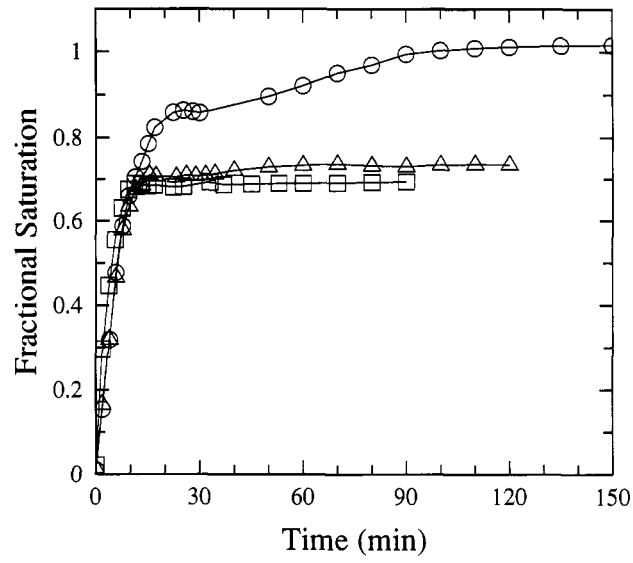

FIGURE 5: Effect of PEG concentration and metheme content on stability and affinity of crystals. The oxygen pressure was changed from 0 to 160 Torr in a single step, and the fractional saturation with oxygen monitored as a function of time at 7 °C. Open circles, crystal with an initial metheme content of 3.0% in 36% (w/v) PEG and 10 mM potassium phosphate, pH 7.3; squares, crystal with an initial metheme content of 3.0% in 54% (w/v) PEG and 10 mM potassium phosphate, pH 7.3; triangles, crystal with an initial metheme content of 14.3% in 36% (w/v) PEG and 10 mM potassium phosphate, pH 7.3.

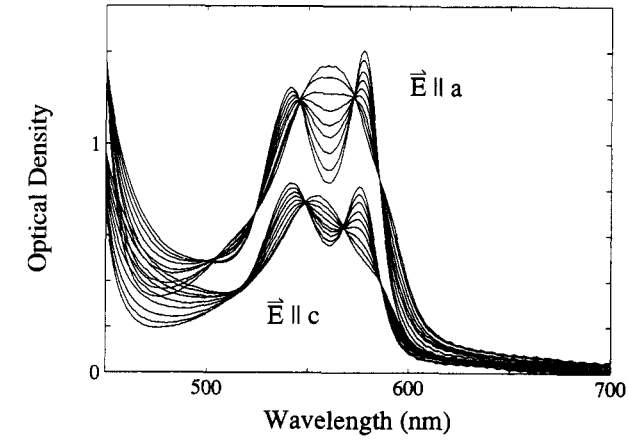

FIGURE 6: Polarized absorption spectra at increasing oxygen pressures. The polarized absorption spectra of a crystal at 15 °C and pH 7.2 [10 mM potassium phosphate and 62% (w/v) PEG] are shown at nine oxygen pressures between 0 and 760 Torr. The upper set of spectra are for linearly polarized light incident normal to the *ac* (010) crystal face with the electric vector parallel to the *a* crystal axis. The lower set of spectra are for light polarized parallel to the *c* crystal axis.

that there is only a single oxyheme spectrum and a single deoxyheme spectrum, with no intermediate spectra. In crystal spectra the presence of isosbestic points has the additional significance that there is only one orientation for the oxyhemes and one orientation for the deoxyhemes. The slight deviation from perfect isosbestic points results from the change in the fraction of methemes (vide infra) and small baseline offsets during the course of the experiment, which required 20 h to complete.

Figure 7 shows the fits of the deoxyHb, oxyHb, and metHb reference spectra to the observed spectra. It is generally not possible to distinguish between the observed and fitted spectra because the agreement is so good. In Figure 8 the fractional saturation with oxygen and the fraction of methemes are plotted versus the oxygen pressure. Throughout this work the fractional saturation with oxygen is defined as the fractional saturation of the reduced (ferrous) hemes, i.e., the fraction of oxyhemes divided by the sum of the fraction of oxyhemes plus deoxyhemes (eq 18). The fraction of methemes was initially 2% and increased approximately linearly in time during the course of the experiment to 14%. The data for increasing oxygen pressure fall on the same curve as the data for decreasing oxygen pressure, demonstrating the complete reversibility of the binding curve. The saturations with oxygen and fraction of methemes calculated from the data for the two polarizations are slightly different, with the *c*-axis data showing higher saturations and more oxidation. Figure 9 shows a Hill plot of the data in Figure 8. For both axes the data fall very close to a straight line with a slope of 1.0, i.e., 0.99 ± 0.01 for the *a* axis and 0.99 ± 0.01 for the *c* axis.

The reversibility of the binding curve not only is important for satisfying the equilibrium criterion but also indicates that formation of methemes has no effect on the binding curve. This was confirmed in a separate series of experiments which showed that the saturation at fixed oxygen pressures is independent of the fraction of methemes (Figure 10). The data in Figure 10 were collected at several pH's in different buffers and show that the saturation is also independent of pH and chloride ion concentration.

Since determining the pH dependence of the oxygen affinity was a major goal of this study, we investigated it in some detail. A question that immediately arises is whether the pH inside the crystal is the same as the measured pH in the solution bathing the crystal. To address this question we measured the pH of a very concentrated hemoglobin solution containing no PEG and the pH of a PEG-containing solution separated from the hemoglobin by a semipermeable membrane. The hemoglobin solution was 35% (w/v) oxyHb, 50 mM Tris, and 0.1 M NaCl, pH 8.1, the PEG-containing solution was 62% (w/v) PEG 8000, 50 mM Tris, and 0.1 M NaCl, pH 8.1, and the semipermeable membrane was benzoylated dialysis membrane. This membrane allows for free diffusion of molecules with molecular weight less than 1200 and is, therefore, impermeable to both PEG and hemoglobin. The difference in pH between the two compartments remained less than 0.05 for about 1 h, at which time measurements were no longer possible due to the onset of precipitation of the hemoglobin.

Two series of binding curves as a function of pH were determined. One series used the 10 mM potassium phosphate buffer and room temperature (21 °C) of the crystallographic studies (Grabowski et al., 1978; Liddington, 1986). The second series was carried out in the 50 mM bis-Tris or Tris buffers containing 0.1 M NaCl at 25 °C. These latter buffers were employed in extensive studies of the pH dependence of the affinity of the T quaternary structure in solution, assumed to correspond to the affinity of the tetramer for the first oxygen molecule (Lee et al., 1988). In preparing the buffer for the crystal experiments, the final concentrations were lower than in the solution experiments, to account for the fraction of the solution volume occupied by PEG which is assumed not to enter the crystal (McPherson, 1976, 1985, 1990). Figure 11 shows Hill plots of the second series. Reversibility was confirmed by remeasuring the saturation in standard air at the end of most experiments. At every pH the Hill plots are linear with a slope very close to 1.0. Figure 12 shows the $p50$ and n as a function of pH.[2] Also shown is the $p50$ as a function of pH from the work of Lee et al. (1988) for the binding of the first oxygen molecule to hemoglobin in solution. The striking result is that, in contrast to solution, the $p50$ is independent of pH. Also, the $p50$ for the crystal is much higher than that for the binding of the first oxygen molecule in solution. The same results were found in potassium phosphate buffer (data not shown).

The lack of a pH dependence was confirmed in experiments on the saturation as a function of pH at constant oxygen pressure. Figure 13 shows the results.[2] Also shown in Figure 13 is the saturation as a function of pH calculated from the binding constant for the first oxygen molecule at an oxygen pressure of 31 Torr. The experiments on the crystal were carried out in three different buffers, 10 mM potassium phosphate, 50 mM Tris/0.1 M NaCl, and 50 mM bis-Tris/0.1 M NaCl. The saturation in all three buffers is very similar. The lack of a chloride effect was confirmed in a separate experiment in bis-Tris at pH 7.4 and 21 °C, shown in Figure 14.

A consistent observation for all of the binding curves measured in the course of these studies was that the $p50$ determined from the data for the *a* crystal axis is always slightly higher than the $p50$ for the *c*-axis data. Table II shows the saturation at a fixed oxygen pressure on 32 different crystals under near X-ray crystallographic conditions where the saturation is 54–55%. The ratio of the *c*-axis saturations to the *a*-axis saturations is 1.04 ± 0.01. The ratio of the $p50$'s ($p50_a/p50_c$) is 1.09 ± 0.04. The α hemes make a greater projection onto the *c* crystal axis, while the α and β heme projections onto the *a* crystal axis are almost the same (Figure 2, Table I). Therefore, the $p50$ of the α hemes is less than that of the β hemes.

A quantitative estimate of the difference in saturations of the α and β hemes can be made using the optical theory described in the Materials and Methods. If it is assumed that the α and β hemes are oxidized to the same extent, then the α and β heme saturations and $p50$'s can be calculated from the *a*-axis and *c*-axis saturations and $p50$'s using analytic expressions (eqs 12 and 13). A more exact calculation can be performed, which takes into account the difference in the fraction of oxidized α and β hemes, using least-squares fitting to the observed spectra (eqs 8–10). Assuming a noncooperative binding curve, the $p50$'s were calculated from these saturations (eq 14). The ratios of the saturations and $p50$'s are greater for the more exact calculation, since there is more oxidation in the α hemes, making the contribution of the α hemes to the binding curve less than is assumed in the more approximate calculation. These calculations suggest that the affinity of the α hemes is about 5 times greater than that of the β hemes.

[2] The slight differences in the data reported in Figure 3 of Mozzarelli et al. (1991) and those in Figures 12 and 13 are due to the use of improved reference spectra in the present study.

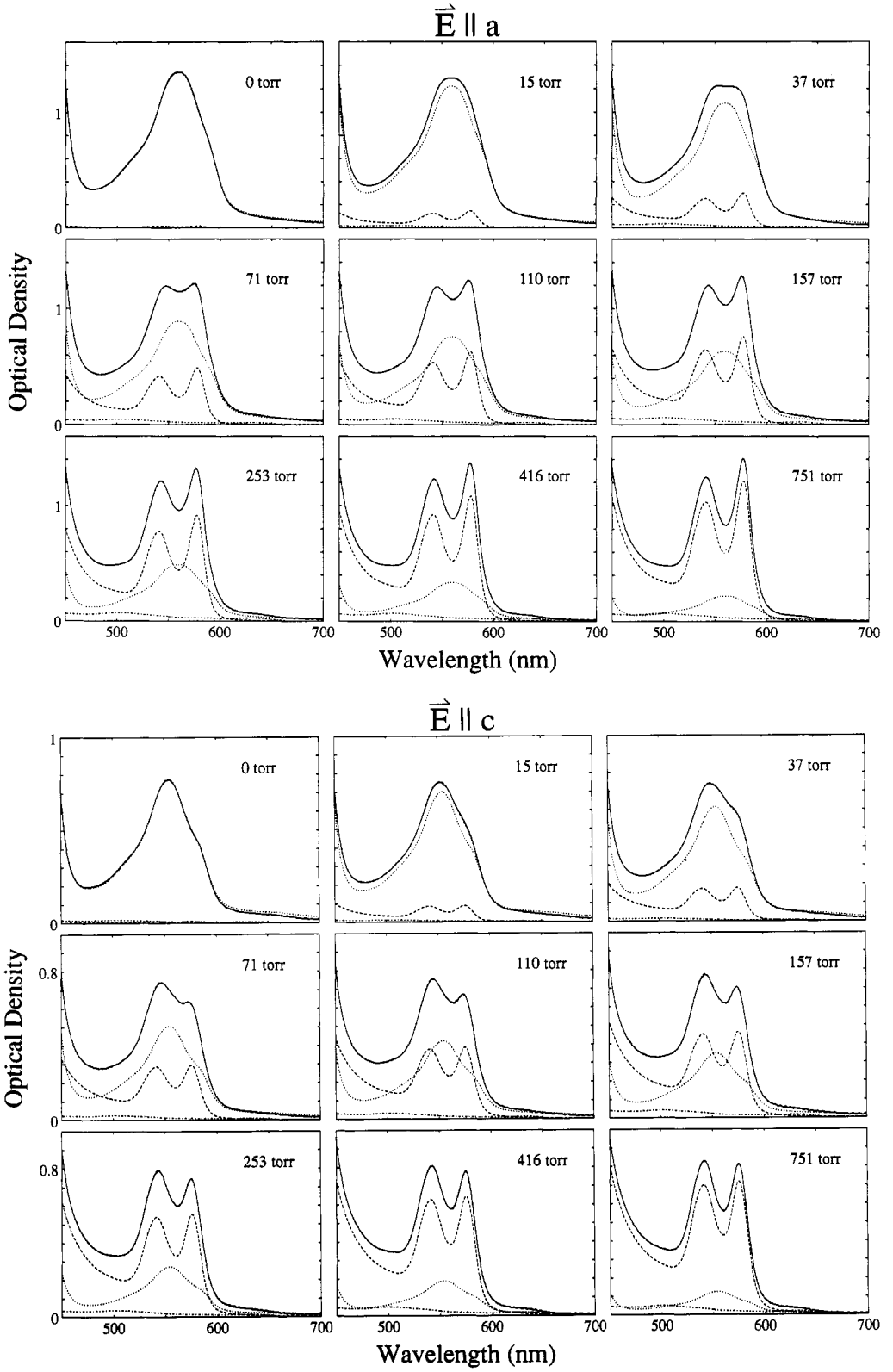

FIGURE 7: Fits of the observed spectra with a linear combination of oxyHb, deoxyHb, and metHb reference spectra. (Top) Spectra measured with light polarized parallel to the *a* crystal axis. (Bottom) Spectra measured with light polarized parallel to the *c* crystal axis. The measured spectra are the continuous curves and the dashed curves are the sum of the component spectra that result from fitting the measured spectra to a linear combination of oxyHb, deoxyHb, and metHb reference spectra. The fits are so good that the dashed curves are barely visible in only a few of the spectra. The components used in the fits are also shown. The dotted curve is the deoxyHb component, the dashed curve is the oxyHb component, and the dashed–dotted curve is the metHb component.

Figure 15 shows complete binding curves for the α and β subunits, where the saturations at each pressure were calculated from eqs 8–10. The sum of these two binding curves gives the binding curve of the tetramer in the crystal, subject to the assumptions used in deriving eqs 8–10. The Hill n for the tetramer binding curves is 1.01 ± 0.04. In this data as well, the ratio of the $p50$'s is about 4 (3.7 ± 0.4).

A series of experiments were carried out to investigate the temperature dependence of the oxygen affinity. The temperature dependence of the oxygen affinity is shown in a van't

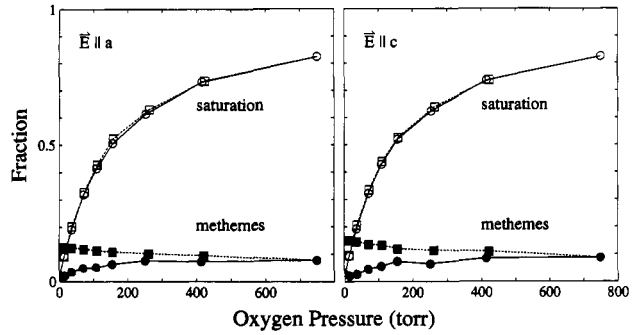

FIGURE 8: Fractional saturation versus oxygen pressure showing reversibility of the binding curve. Fractional saturation of reduced hemes with oxygen (open symbols) and fraction of methemes as a function of oxygen pressure (filled symbols) for data measured along the *a* (left panel) and *c* (right panel) crystal axes. These are the results of the fits to the spectra of the experiment shown in Figure 7. The fractional saturation with oxygen is defined as the fractional saturation of the reduced (ferrous) hemes, i.e., the fraction of oxyhemes divided by the sum of the fraction of oxyhemes plus deoxyhemes (eq 18). The circles (connected by continuous lines) are calculated for the data at increasing oxygen pressures and the squares (connected by dashed lines) are calculated for the data from decreasing oxygen pressures.

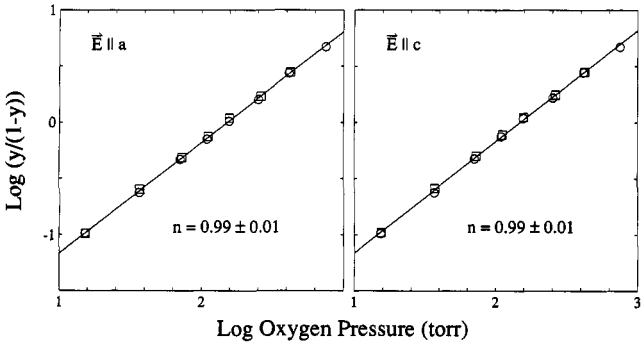

FIGURE 9: Hill plots of data in Figure 8 showing noncooperativity of the binding curve. (Left) Data from *a* crystal axis. (Right) Data from *c* crystal axis. The circles are calculated from the data for increasing oxygen pressure and the squares from the data for decreasing oxygen pressure. The lines through the data are least-squares fits which result in $n = 0.99 \pm 0.01$ and $p50 = 155 \pm 1$ Torr for the *a*-axis data and $n = 0.99 \pm 0.01$ and $p50 = 141 \pm 1$ Torr for the *c*-axis data.

Hoff plot (Figure 16). The ΔH calculated from the $p50$'s is -13.3 ± 0.8 kcal/mol of O_2; this is the ΔH for the reaction Hb(crystal) + O_2(gas) → HbO_2(crystal). Imai (1979) determined a ΔH of -12.1 kcal/mol from van't Hoff plots for binding the first, gas-phase oxygen molecule to hemoglobin in solution at 25 °C in 0.1 M NaCl at pH 7.4. After correcting for the heat of proton and chloride ion binding (Antonini et al., 1965), he calculated an intrinsic ΔH for binding the first oxygen molecule from the gas phase of -18.1 kcal/mol (Imai, 1979; Chu et al., 1984). The calculated entropy and free energy changes are also given in Table III.

DISCUSSION

Several novel and important results have emerged from this study. At low PEG concentration and low fraction of methemes, crystals of deoxyHb crack upon oxygenation and show a time-dependent increase in affinity, which we tentatively interpret as signaling the conversion of the quaternary structure from T to R (Figure 5). If, however, the PEG concentration and/or the fraction of methemes is sufficiently high, crystals grown as deoxyHb undergo perfectly reversible oxygenation. The demonstration in Figures 8 and 9 that the binding curve obtained by increasing the oxygen pressure is

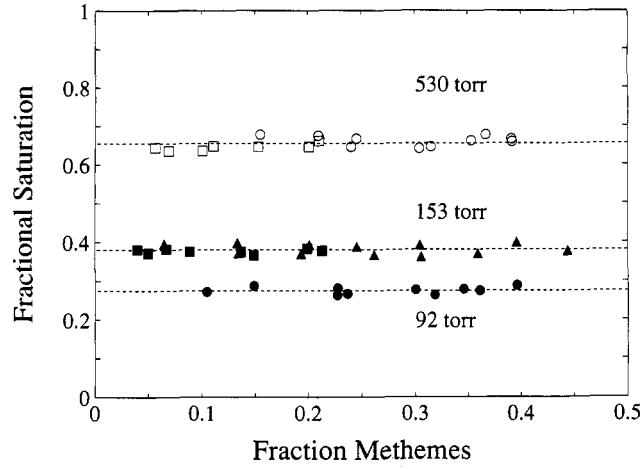

FIGURE 10: Effect of oxidation on oxygen affinity. The fractional saturation with oxygen is plotted versus the fraction of methemes. The data were obtained by exposing crystals to a constant oxygen pressure at 25 °C and by measuring the spectra as a function of time for periods up to 10 h. (□) 530 Torr, pH 7.2–7.4, 10 mM potassium phosphate and 62% (w/v) PEG; (○) 530 Torr, pH 7.0–7.2, 10 mM potassium phosphate and 62% (w/v) PEG; (▲) 153 Torr, pH 7, 50 mM Tris, 0.1 M NaCl, and 62% (w/v) PEG; (■) 153 Torr, pH 8.0, 50 mM bis-Tris, 0.1 M NaCl, and 62% (w/v) PEG; (●) 92 Torr, pH 6.5, 50 mM bis-Tris, 0.1 M NaCl, and 62% (w/v) PEG.

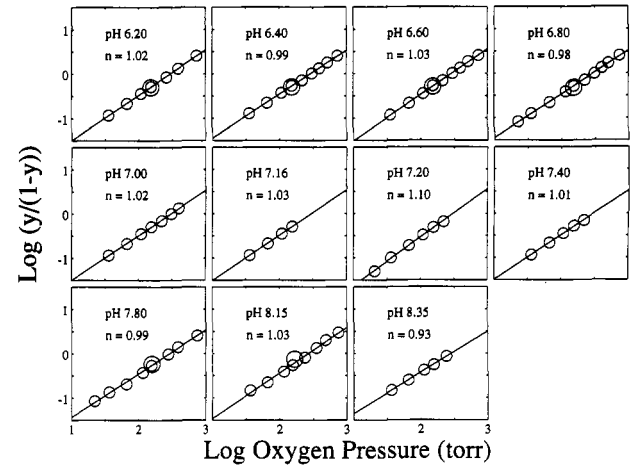

FIGURE 11: Hill plots of binding curves between pH 6.0 and 8.4 at 25 °C. For pH's 6.20, 6.40, 6.60, 6.80, 7.00, 7.16, 7.20, and 7.40, the buffer was 50 mM bis-Tris:HCl containing 0.1 M NaCl and 36% (w/v) PEG. For pH's 7.80, 8.15, and 8.35, the buffer was 25 mM Tris containing 0.05 M NaCl and 62% (w/v) PEG. The large circles correspond to the saturation obtained at the end of the experiment, indicating reversibility of the binding curve. The higher PEG concentration used for the more alkaline pH's was necessary to prevent cracking of the crystals. The saturations were determined from the spectra measured with light polarized parallel to the *c* axis.

identical to that obtained by decreasing the oxygen pressure is of course the essential criterion for establishing that a true equilibrium binding curve was being measured. Under these conditions the crystal binding curve is apparently noncooperative, with an oxygen affinity that is the lowest yet observed for normal human hemoglobin (Figure 9). Perhaps the most striking result is that the oxygen affinity of the crystal is unaffected by changes in pH (Figures 12 and 13). Because the α and β hemes have different orientations in the crystal and therefore contribute differently to the polarized spectra, there is additional information in crystal experiments that is not obtainable from experiments on solutions. By comparing the results determined from the spectra with light polarized parallel to the two different crystal axes, we have estimated that the $p50$ for the α hemes is about 5-fold smaller than that

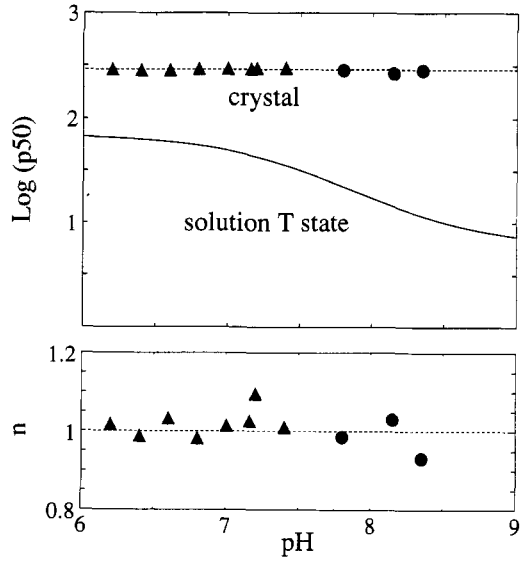

FIGURE 12: Comparison of pH dependence of oxygen affinity in solution and in the crystal at 25 °C. (Top) Log $p50$ versus pH. The points are the $p50$'s from Figure 11 and the curve is the data of Lee et al. (1988) for the binding of the first oxygen molecule to hemoglobin, $4/K_{41}$ [the statistical factor of 4 was inadvertently missing from the label to Figure 2a in Lee et al. (1988)]. (Bottom) n versus pH. These are the slopes of the Hill plots from the data in Figure 11.

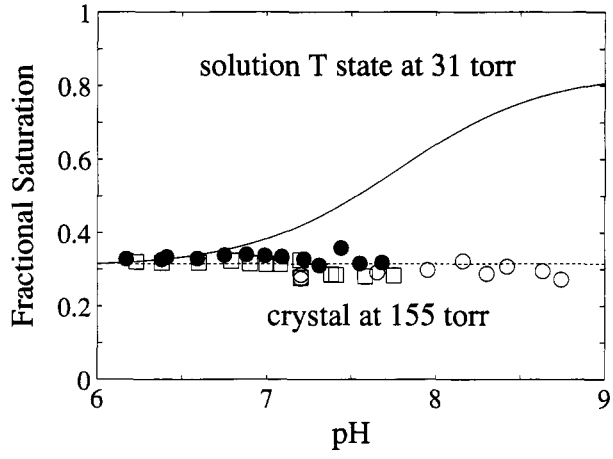

FIGURE 13: Saturation versus pH at constant oxygen pressure (standard air, 155 Torr of oxygen) and 25 °C. The open circles are the measured fractional saturations in 25 mM Tris:HCl buffer containing 0.05 M NaCl [62% (w/v) PEG]; the fraction of methemes in these experiments ranged from 0.07 to 0.23. The filled circles are the measured fractional saturations in 50 mM bis-Tris:HCl buffer containing 0.1 M NaCl [36% (w/v) PEG]; the fraction of methemes in these experiments ranged from 0.13 to 0.52. The squares are the measured fractional saturations in 10 mM potassium phosphate buffer [36% (w/v) PEG]; the fraction of methemes in these experiments ranged from 0.1 to 0.35.

of the β hemes (Figure 15, Table II), in marked contrast to the X-ray findings that only the α hemes bind oxygen. We shall see that this difference in affinity is almost exactly compensated by a small amount of cooperativity to produce an apparently perfectly noncooperative tetramer. Since the fractional oxygenation of the reduced hemes is unaffected by oxidation (Figure 10), none of the above results are affected by the fact that there was, unavoidably, significant oxidation during the course of the experiments. That is, the intrinsic affinity of the tetramer for oxygen is independent of the number of oxidized as well as oxygenated hemes.

The stabilizing effect of methemes is not unexpected. MetHb in the present crystal lattice is stable in the T quaternary structure and its structure has been determined

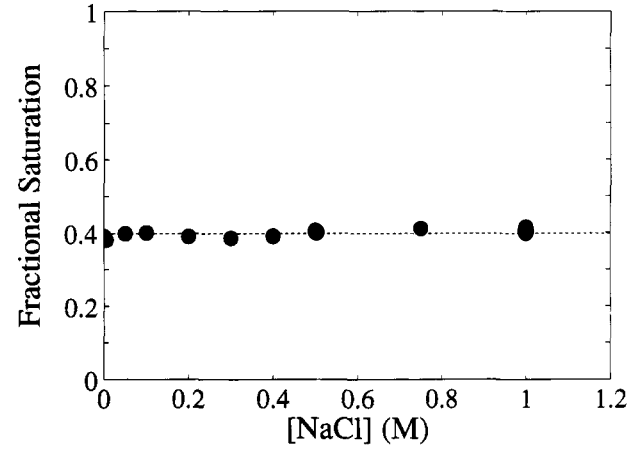

FIGURE 14: Effect of sodium chloride concentration on oxygen saturation at 154 Torr at 21 °C. This experiment was carried out in 25 mM bis-Tris buffer at pH 7.4 in 62% (w/v) PEG.

Table II: Multiple Determinations of α and β Heme Saturations in Air at 15 °C[a]

	Observed[b] fractional saturation	$p50$[c] (Torr)
a axis	0.527 ± 0.014	140 ± 8
c acis	0.549 ± 0.021	129 ± 10
ratio	1.040 ± 0.015	1.09 ± 0.04

	Calculated fractional saturation		$p50$ (Torr)	
	method I[d]	method II[e]	method I[f]	method II[f]
α hemes	0.66 ± 0.06	0.70 ± 0.05	82 ± 21	68 ± 16
β hemes	0.40 ± 0.03	0.37 ± 0.04	239 ± 44	275 ± 53
ratio	1.7 ± 0.4	1.9 ± 0.4	3.4 ± 2.3	4.5 ± 2.2

[a] 156 Torr of oxygen, 10 mM potassium phosphate buffer, pH 7.3, and 62% (w/v) PEG. Only the wavelength regions 525–580 and 630–650 nm were included in these determinations. [b] The results are the average of measurements made on 32 different crystals. The uncertainties are standard deviations from the mean value. In these experiments the average metheme content was 4%, with a range of 0–8%. [c] Calculated from the Hill equation with $n \approx 1$. [d] Calculated from eqs 12 and 13. [e] Calculated from eqs 8–10. [f] Calculated from saturations using eq 14.

to high resolution (Liddington et al., 1988; Perutz et al., 1987). Furthermore, it is known from biochemical studies that oxidation of hemoglobin in solution has a smaller effect on favoring the R quaternary structure over the T quaternary structure than does oxygenation (Perutz et al., 1974, 1976). Additional support for this conclusion comes from an interesting observation made in X-ray diffraction studies on crystals of deoxyHb grown from concentrated salt solution. Oxygenation resulted in loss of most of the diffraction pattern of these crystals, presumably due to the T to R conformational change, while oxidation of the crystals resulted in metHb in the T quaternary structure diffracting to better than 0.35 nm (Anderson, 1973).

There are several lines of evidence, in addition to the finding of a reversible, noncooperative binding curve, to indicate that hemoglobin in intact crystals remains in the T quaternary structure at all oxygen saturations. First, the X-ray diffraction measurements under one set of conditions at partial oxygenation [36% (w/v) PEG and 10 mM potassium phosphate, pH 7.0 ± 0.2, air, room temperature, unknown fraction of methemes] show that the quaternary structure is T (Brzozowski et al., 1984a; Liddington, 1986; Liddington et al., 1988). Second, the polarization ratio for the fully oxygenated crystal is in close agreement with that expected from the available X-ray structural information on liganded molecules in the T quaternary structure (Table I). The difference in the

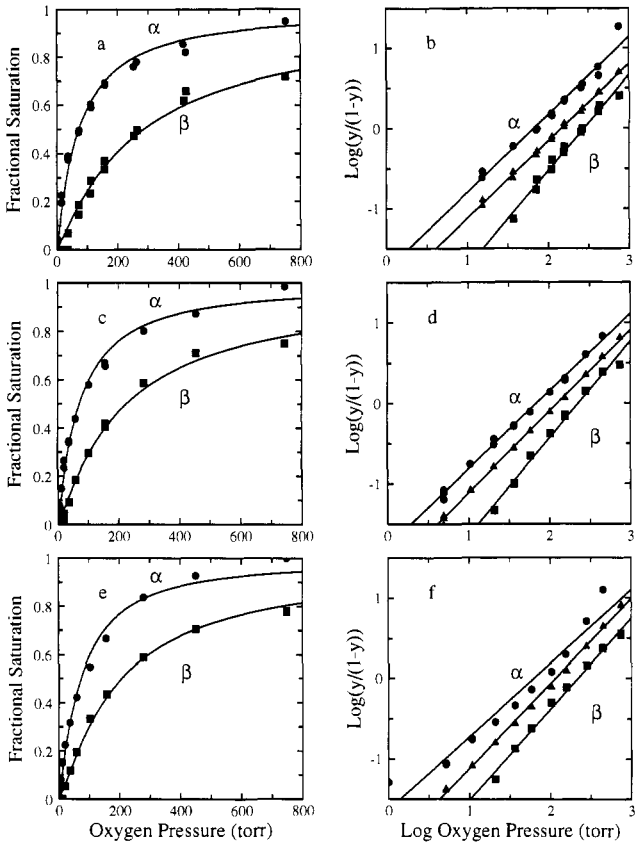

FIGURE 15: Separate binding curves for α and β hemes. The saturations were calculated from eqs 8–10. The tetramer binding curve was calculated from the sum of the α and β binding curves. To the extent that the calculations of the α and β binding curves are correct, this is the binding curve for the tetramer in the crystal. The slopes in the Hill plots for the tetramer binding curves (triangles) are 0.96 ± 0.01, 1.01 ± 0.01, and 1.05 ● 0.02 for panels b, d, and f, respectively. The curves through the data in panels a, c, and e were obtained from a least-squares fit using the equations for a cooperative dimer (eq 21). (a, b) From the data of the experiment shown in Figure 6. (c, d) and (e, f) Same conditions as the experiment of Figure 6.

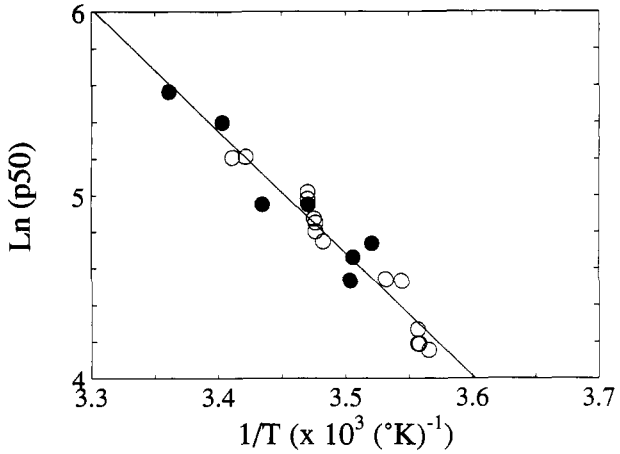

FIGURE 16: van't Hoff plot of $p50$. The $p50$'s are the average of the data for the *a* and *c* crystal axes. (○) 10 mM potassium phosphate, pH 7.2, and 36–62% (w/v) PEG; (●) 50 mM bis-Tris, 0.1 M NaCl, pH 7.4, and 62% (w/v) PEG. The ΔH, calculated from the slope using the van't Hoff relation, d ln $p50$/d $(1/T) = \Delta H/R$, is −13.3 ± 0.8 kcal/mol.

polarization ratios for the fully deoxygenated and the fully oxygenated crystal (Table I) indicates that there is a change in the β heme orientation upon oxygen binding. Since the heme is tightly packed inside the protein, the change in heme

Table III: Comparison of Apparent Thermodynamic Parameters for Oxygen Binding by Hemoglobin in Crystal and Solution at 25 °C and pH 7.4

	$p50$ (Torr)	ΔG^a (kcal/mol)	ΔH^b (kcal/mol)	$T\Delta S^c$ (kcal/mol)
crystal[d]	286 ± 15	−0.58 ± 0.03	−13.3 ± 0.8	−12.7 ± 0.8
solution[e]	46[f]	−1.7	−12.1 (−18.1[g])	−10.4

[a] Calculated from $\Delta G = -RT \ln (1/p50)$, using a standard state for gaseous oxygen of 760 Torr. [b] Calculated using the van't Hoff relation. [c] Calculated from the relation $T\Delta S = \Delta H - \Delta G$. [d] From the data in Figure 15. [e] From Imai (1979). [f] $p50 = 1/K_1$, where K_1 is the intrinsic association constant for the binding of the first oxygen molecule to the tetramer and is a very good approximation to the T-state affinity in a two-state allosteric model (Imai, 1982). [g] Corrected by Imai (1979) for the heat of proton and anion binding (Antonini et al., 1965).

orientation is accompanied by a change in tertiary conformation of the surrounding globin.[3]

Finally, additional evidence that the quaternary structure remains T is provided by the quality of the fits of the observed spectra with the metHb, deoxyHb, and oxyHb reference spectra. The fits are so good that there is no indication of any intermediate spectral species (Figure 5), suggesting that there are only liganded and unliganded protein conformations. Intermediate deoxyheme spectra are observed in solution, presumably due to partially oxygenated molecules in the R quaternary structure (Ownby & Gill, 1990). Changes in heme orientation in the crystal accompanying a T to R quaternary conformational change could change the crystal extinction coefficients (eq 5) and thereby remove the isosbestic points. Table IV compares the absorption ellipsoids of hemoglobin in the R and T quaternary structures. Surprisingly, the principal extinction coefficients of the absorption ellipsoids of the R and T conformations are very similar for oxyHb, deoxyHb, and metHb. There is, however, a rotation of $\alpha\beta$ dimers relative to each other by about 15°, with a corresponding rotation of the dyad (y) molecular axis by about 7.5°. Consequently, it is not possible to predict the change in the crystal extinction coefficients accompanying a T to R conformational change without a detailed model for the orientation of the R quaternary structure in the crystal lattice.

In the following we discuss the significance of each of the major results of the measurements of oxygen binding to the

[3] Makinen and Eaton (1974) and Eaton and Hofrichter (1981) observed changes in polarization ratios in the Soret spectral region upon oxidation, as well as upon both oxygen and carbon monoxide binding to the R quaternary structure, which they interpreted as resulting from a change in heme orientation. A tilt of both the α and β hemes and the associated conformational change upon oxidation of deoxyHb in the R quaternary structure to metHb in the R quaternary structure has recently been confirmed by X-ray crystallography (Perutz et al., 1987; Luisi et al., 1990; B. Luisi, unpublished results). The agreement between the X-ray and optical data is remarkably good. The X-ray coordinates show a 2.0° tilt for the α hemes and a 3.3° tilt for the β hemes, while the optical data predict a minimum average tilt of 2.6° ± 0.4° (Makinen & Eaton, 1974; Eaton & Hofrichter, 1981). The similarity of the observed polarization ratios for the fully oxygenated molecule in the T quaternary structure and those predicted from the structure of the liganded T-state molecule, $\alpha(Ni)_2\beta(FeCO)_2$, suggests that the heme orientations, and therefore the tertiary conformations, of the β subunits are similar. Luisi et al. (1990) have suggested that the translation and rotation of the β hemes relieves steric interference with carbon monoxide by the distal residues, particularly valine E11. It would, therefore, be somewhat surprising if the conformational changes associated with oxygen binding were *identical*; the steric interference with oxygen is expected to be less than that of carbon monoxide, since the Fe–O–O bond angle should be considerably more acute than that of Fe–C–O (Shaanan, 1983; Perutz et al., 1987). Some small differences in the structure of the oxy and carbonmonoxy β subunits may also be expected because the space groups of the crystals are different, resulting in different effects of intermolecular contacts on the conformations.

Table IV: Absorption Ellipsoids of Oxyhemoglobin, Deoxyhemoglobin, and Methemoglobin in the R and T Quaternary Structures[a]

molecule	ϵ_x	ϵ_y	ϵ_z
R oxyhemoglobin[b]	$0.39\bar{\epsilon}$	$1.13\bar{\epsilon}$	$1.48\bar{\epsilon}$
T oxyhemoglobin[c]	$0.39\bar{\epsilon}$	$1.12\bar{\epsilon}$	$1.50\bar{\epsilon}$
R deoxyhemoglobin[d]	$0.33\bar{\epsilon}$	$1.19\bar{\epsilon}$	$1.48\bar{\epsilon}$
T deoxyhemoglobin[e]	$0.33\bar{\epsilon}$	$1.17\bar{\epsilon}$	$1.49\bar{\epsilon}$
R methemogobin[f]	$0.35\bar{\epsilon}$	$1.16\bar{\epsilon}$	$1.49\bar{\epsilon}$
T methemoglobin[g]	$0.37\bar{\epsilon}$	$1.14\bar{\epsilon}$	$1.49\bar{\epsilon}$

[a] The absorption ellipsoid was calculated using eq 5 (with $cl = 1$), where the μ directions now refer to axes in the molecular frame, rather than crystal axis directions. The molecular axes were constructed using the following prescription (Fermi & Perutz, 1981): the y molecular axis was chosen to be the true molecular dyad axis. For those X-ray structures which do not possess a true 2-fold axis relating the $\alpha_1\beta_1$ and $\alpha_2\beta_2$ dimers, the approximate molecular dyad axis was constructed by symmetry-averaging the structure (averaging the original coordinates with a set of coordinates produced by least-squares superposition onto the original structure of all heavy atoms of the molecule with the $\alpha\beta$ dimers interchanged) and performing a second superposition of the original structure onto the molecule produced by interchanging the dimers, using only those atoms which in the original structure are displaced by less than 0.1 Å from their positions in the symmetry-averaged structure; the axis of rotation for the latter superposition is chosen as the molecular dyad axis. The x molecular axis is then constructed by projecting onto the plane perpendicular to the dyad axis the bisector of the angle between the vectors connecting the center-of-mass of the four heme irons with the α_1 and β_1 heme irons. The z axis is the vector outer product of the x and y molecular axes. The angles $z_i\mu$ in eq 5 are the angles between the heme normals and one of these axes. [b] From the structure by Shaanan (1983), in which the molecular and crystal dyads coincide. [c] From the structure produced from the α subunits of semioxyhemoglobin (Liddington et al., 1988) and the β subunits of the nickel–iron hybrid hemoglobin $\alpha(Ni)_2\beta(FeCO)_2$ (Luisi et al., 1990), oriented as described in Table I. The final superposition for producing the molecular dyad axis included 607 atoms/subunit dimer. [d] From the structure of horse BME deoxyHb (B. Luisi, unpublished results), in which the molecular and crystal dyads coincide. [e] From the $P2_12_12$ deoxyHb structure of Liddington (unpublished results). The superposition to produce the molecular dyad included 692 atoms/subunit dimer. [f] From the structure of horse metHb (BNL file 2MHB), in which the molecular and crystal dyads coincide. [g] From the $P2_12_12$ metHb structure of Liddington (unpublished results). The superposition to produce the molecular dyad included 795 atoms/subunit dimer.

crystals for understanding the mechanism of cooperative oxygen binding. We shall see that it is possible to understand the relation between the X-ray structural information and the oxygen binding properties of the crystal with relatively model-free considerations. On the other hand, the discussion of the relation between the crystal results and the results on hemoglobin in solution is much more model-dependent.

The Absence of a Bohr Effect in the Crystal Is Consistent with Perutz's Salt Bridge Hypothesis. A striking feature of the crystal results is that the pH dependence of the oxygen affinity is very different from that of the T quaternary structure in solution. Over the range where the crystal affinity is unaffected by pH (Figures 12 and 13), the $p50$ for the T quaternary structure of hemoglobin in solution, assumed to correspond to the affinity of the tetramer for the first oxygen molecule, changes by a factor of 7. The observation of a pH-independent binding curve in the crystal is consistent with the existing X-ray crystallographic data. In addition to the crystal that we have studied, which shows intact salt bridges upon partial oxygenation (Brzozowski et al., 1984a; Liddington et al., 1988), there are X-ray studies on crystals of several metal hybrids which also show intact salt bridges for α subunits in the T quaternary structure that are fully liganded with carbon monoxide (Arnone et al., 1986; Perutz et al., 1987; Luisi & Shibayama, 1989; Luisi et al., 1990; Abraham et al., 1992). This is also true for the β-liganded molecule in the T quaternary structure, $\alpha(Ni)_2\beta(FeCO)_2$ (Luisi, personal communication). Furthermore, there are no structural changes that would suggest a change in pK of an ionizable group upon ligation (Luisi & Shibayama, 1989).

The lack of a Bohr effect in the crystal is thus consistent with Perutz's stereochemical mechanism in which oxygen binding causes rupture of the salt bridges and release of protons (Perutz, 1970) (Figure 1). This conclusion of course rests on the assumption that the salt bridges remain intact over the entire pH range of our measurements. Breakage of the salt bridges in the crystal without a Bohr effect would require a conformational change that results in the binding of the same number of protons that are released by the residues involved in the salt bridges—an unlikely occurrence. At some alkaline pH, however, we would expect to observe the dissociation of protons and rupture of the salt bridges. The question is whether the molecules in the crystal would remain in the T quaternary structure. It is interesting in this regard that we have observed an increase in affinity of the crystal at pH's greater than 9 (data not shown), where cracks develop. It is not clear, however, whether the conformational changes that disrupt the crystal are changes within a T quaternary structure or represent a T to R quaternary conformational change. Luisi and Shibayama (1989) have pointed out that the finding of intact salt bridges suggests that the tertiary conformational change responsible for the Bohr effect within the T quaternary structure is a global conformational change. If this were true, it is possible that crystals may develop cracks upon oxygenation without a change in quaternary structure. More detailed binding, as well as X-ray studies, on crystals at very alkaline pH's would be worthwhile.

The Low Affinity and Absence of a Bohr Effect Suggest an Interesting Generalization of the MWC–PSK Model. The most obvious interpretation of the lack of a Bohr effect in the crystal is that the Bohr effect requires a change in quaternary structure, as envisaged in the original MWC model (Monod et al., 1965). However, this interpretation would make it impossible to explain the pH dependence for the binding of the first oxygen molecule to the tetramer, the so-called "tertiary" Bohr effect, using an MWC–PSK-type model (Johnson et al., 1984; Lee et al., 1988). There is an alternative interpretation, which explains the low affinity of the crystal as well as the difference in the pH dependence of oxygen binding to the T quaternary structure between crystal and solution yet retains the basic features of the MWC–PSK model (Figure 1). In this model individual subunits have two affinity states in the T quaternary structure (Figure 17). The high-affinity state corresponds to the tertiary conformation with broken salt bridges, while the low-affinity state corresponds to the tertiary conformation with unbroken salt bridges. In both crystal and solution the tertiary conformation with unbroken salt bridges is more stable for a deoxygenated subunit in the T quaternary structure. For an oxygenated subunit, the tertiary conformation with unbroken salt bridges is also more stable in the crystal, but the tertiary conformation with broken salt bridges is more stable in solution. The breakage of the salt bridges in solution upon oxygenation releases protons, accounting for the tertiary Bohr effect, while no such breakage occurs in the crystal with the result that the affinity is lower and there is no Bohr effect (an equivalent description is that the affinity of the T quaternary structure in the crystal is lower because the lattice forces prevent the tertiary conformational change that partially relieves the strain in the liganded structure). As long as the breakage of the salt bridge does not affect the affinity of the adjacent subunit to which the salt bridge is attached, binding will be noncooperative.

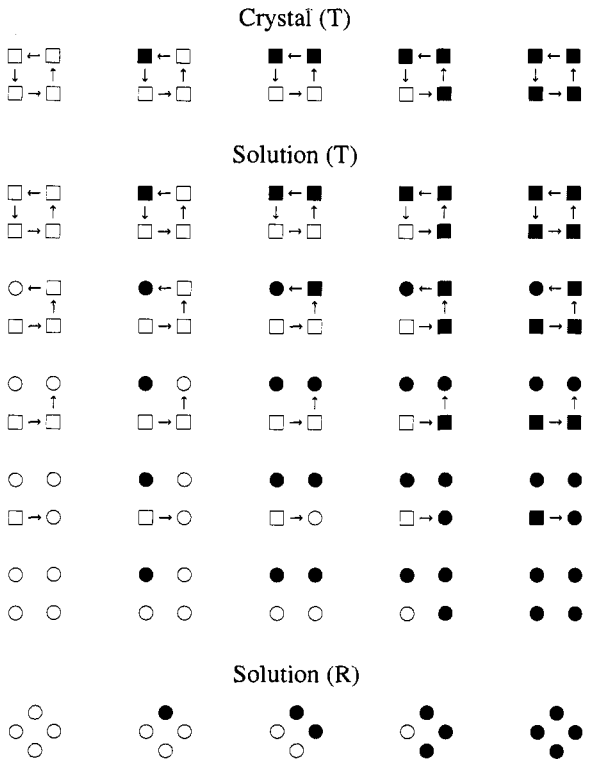

FIGURE 17: Comparison of binding to T quaternary structure in crystal and in solution. As in Figure 1, this is a simplified diagram of the relation between the salt bridges, tertiary conformation, and ligation state within the T quaternary structure. The squares designate the low-affinity conformation with unbroken salt bridges, while the circles designate the high-affinity conformation with broken salt bridges. Open symbols correspond to unliganded subunits, while filled symbols correspond to liganded subunits. In the crystal, only the conformation with unbroken salt bridges is populated, binding occurs without rupture of the salt bridges, and there is no Bohr effect. In solution all possible combinations of conformations may exist, but the most populated species at neutral pH are those that lie along the diagonal. That is, binding changes the tertiary conformation from one with unbroken salt bridges to one with broken salt bridges, thereby producing a tertiary Bohr effect.

The binding polynomial for this model is (Hess & Szabo, 1979)

$$Q = L\left[\frac{l}{l+1}\right]^4\left[1 + \left(\frac{l}{l+1}K_{Tt} + \frac{1}{l+1}K_{Tr}\right)p\right]^4 + [1 + K_R p]^4 \quad (19)$$

where L is the allosteric equilibrium constant for the quaternary conformational change of the completely unliganded tetramer with all four subunits in the t conformation ($\equiv[Tt_4]/[R]$), l is the equilibrium constant for the tertiary conformational change of the unliganded subunits ($\equiv[Tt]/[Tr]$), K_{Tt} is the binding constant to the low-affinity tertiary conformation in the T quaternary structure with unbroken salt bridges in both unliganded and liganded states, K_{Tr} is the binding constant to the high-affinity tertiary conformation in the T quaternary structure with broken salt bridges in both unliganded and liganded states, K_R is the binding constant to a subunit in the R quaternary structure, and p is the oxygen pressure. Notice that apart from the prefactor the partition function is identical to that for a two-state allosteric model if the composite equilibrium constant, $[l/(l + 1)]K_{Tt} + [1/(l + 1)]K_{Tr}$, is identified with the MWC K_T. In this model the variability in the affinity of the T quaternary structure results from the dependence of l on solution conditions.

We can estimate the $p50$'s at 25 °C for each of the three subunit affinity states, ignoring for simplicity the inequivalence in the α and β subunits (see below). The $p50$ for the low-affinity tertiary conformation of the T quaternary structure (Tt), which corresponds to what is observed in the crystal, is about 300 Torr. The $p50$ for the high-affinity conformation is less than 10 Torr, as judged by the apparent T-state affinity in solution at alkaline pH (Imai, 1982), where we can assume that the salt bridges are broken in the liganded form and partially broken in the unliganded form. The $p50$ for the R state is about 0.3 Torr (Imai, 1982). There remains the possibility that the tertiary conformation with broken salt bridges in the T quaternary structure (Tr) may have the same conformation and affinity as the tertiary conformation in the R quaternary structure, i.e., $K_{Tr} = K_R$ in eq 19. If this were the case, this model would reduce to a two-state model in which there is incomplete coupling of tertiary and quaternary conformations. That is, in the T quaternary structure both a high- and low-affinity tertiary conformation may exist (t and r), while in the R quaternary structure only the high-affinity (r) conformation is populated.

A useful feature of this generalization of the MWC–PSK model is that it may explain the large range of T-state binding constants in solution (Minton & Imai, 1974; Imai, 1982) as resulting from a shift in the equilibrium population of liganded T-state subunits toward the conformation with unbroken salt bridges by allosteric effectors such as chloride and organic phosphates. The lack of a chloride effect in the crystal (Figure 14) is expected, since chloride presumably stabilizes the conformation with unbroken salt bridges which is already 100% populated. Since these effectors may interact with more than one subunit, binding at nonsaturating concentrations in solution will result in cooperative binding. The need for some kind of third affinity state was first recognized by Minton and Imai (1974). Also, the possibility of ligation of subunits in the T quaternary structure without salt bridge breakage was considered by Lee and Karplus (Lee & Karplus, 1983; Lee et al., 1988) (Figure 1).

There are "strong" allosteric effectors which produce $p50$'s for the T-state as high as 210 Torr, comparable to what is observed in the crystal (Lalezari et al., 1990; Marden et al., 1990). The generalized MWC–PSK model of Figure 17 would predict that the low affinity arises from the stabilization of the low-affinity tertiary (Tt) conformation with intact salt bridges for the liganded subunits. A consequence of this is that there should be a much reduced or absent tertiary Bohr effect with these allosteric effectors, as is observed in carp hemoglobin (Tan & Noble, 1973). The model also makes the interesting prediction that the Bohr effect will be reduced under conditions of high affinity of the T quaternary structure, where there is a significant population of unliganded subunits with broken salt bridges (Tr).

In Contrast to the X-ray Result, the β Hemes Also Bind Oxygen. The surprising result from the X-ray studies of Brzozowski et al. (1984a) and Liddington et al. (1988) is that oxygen was observed only bound to the α hemes. In the electron density map the oxygen binding site was fully occupied, and no oxygen was observed bound to the β hemes (Brzozowski et al., 1984a). We can investigate this question from our data at several different levels of detail. First, the observation of oxygen saturations greater than 80% shows unambiguously that the β hemes also bind oxygen. Second, the binding curves (Figures 9 and 12) show no sign of the biphasic behavior that would be expected from the large difference in affinity of the α and β subunits. Furthermore, a linear Hill plot with a slope of unity puts limits on the inequivalence of the affinity of the α and β subunits, if it is assumed that there is no cooperativity.

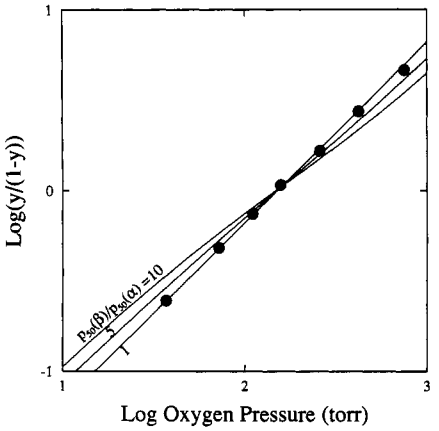

FIGURE 18: Hill plots for noncooperative curves with α,β inequivalence. The filled circles are the averaged a and c axis data from Figure 8. The lines are least-squares fits to these data of the average of the apparent saturations along the two directions from eq 11, where the saturations of the α and β subunits are given by eq 14. The three curves are from fits with the ratio of affinities of the α and β subunits constrained to values of 1, 5, or 10.

Figure 18 compares Hill plots of the data with predicted curves for a noncooperative tetramer with varying ratios of the affinity of the α and β subunits. The linearity of the data in a Hill plot is sufficient to suggest that the ratio of affinities is less than a factor of about 5 (Figure 18).

Finally, we can investigate the question of the difference in affinities of the α and β subunits in detail by taking advantage of the fact that the α and β hemes make different projections onto the two crystal axes (Figure 2, Table I) and therefore make unequal contributions to the measured spectra. The greater contribution of the α hemes to the c-axis spectra, together with the lower $p50$ for the c-axis data, indicates that the α subunits have a higher oxygen affinity than the β subunits. To obtain oxygen saturations we have carried out an analysis that depends on knowing the heme orientations in the deoxy, oxy, and met states and on the fact that the hemes in all three states behave like circular absorbers of linearly polarized light (see Optical Theory). We have also assumed that there is no difference in the saturations of the two α (or two β) subunits even though they have different intermolecular contacts in the crystal. The results of this analysis for a series of crystals under near crystallographic conditions is shown in Table II. At 15 °C and the oxygen pressure of air, the saturation of the α subunits is 70%, while the saturation of the β subunits is 37%. Assuming that binding is noncooperative and that the $p50$'s of the α and β subunits have the same temperature dependence as the overall $p50$ (figure 16), the saturations of the α and β subunits at room temperature are calculated to be 60% and 27%, respectively.

We do not yet fully understand the discrepancy between the optical and X-ray results. Other publications of the X-ray work suggest that the interpretation of the electron density map by Brzozowski et al. (1984a) and Liddington et al. (1988) may have been somewhat oversimplified. Brzozowski et al. (1984b) reported that "no more than 10–20% of the β subunits have bound oxygen"; Perutz et al. (1987) reported that "The refined structure shows full occupancy by O_2 at the α-hemes and no evidence of O_2 bound to the β-hemes, but up to 30% of the β hemes may have become oxidized to methemoglobin (Hb^+H_2O)"; Waller and Liddington (1990) reported, without further comment, that "semioxygenated haemoglobin...had fully occupied oxygen molecules bound to the α hemes and a low level (25%) of ligation at the β hemes".

In any case, all of the analyses of the X-ray data appear to overestimate the fractional oxygenation of the α hemes and underestimate the fractional oxygenation of the β hemes. Also, our results suggest that the crystal in the X-ray diffraction studies may have contained roughly equal amounts of deoxyhemes, oxyhemes, and methemes. A clue to understanding the discrepancy in the results for the α heme occupancy comes from the recent study of Waller and Liddington (1990), who solved the X-ray structure to 0.15-nm resolution of a crystal in air, which was grown in the presence of IHP. They calculated 40% occupancy of the proximal oxygen atom site on the α heme, 100% occupancy of the distal oxygen atom site, and no sign of any ligand on the β hemes. Because the electron density at the distal site can arise from the water molecule of the deoxy form which is hydrogen bonded to the distal histidine, they interpreted the observations on the α heme to represent 40% saturation with the oxygen molecule.[4] Thus it seems quite possible that, in the structure of "semioxyhemoglobin", oxidation to produce electron density at the proximal site from the bound water molecule of the metheme, together with the electron density at the distal site from the water molecule hydrogen bonded to the distal histidine in the deoxy form (Waller & Liddington, 1990), could have been mistaken for electron density from an oxygen molecule.

One possibility for the β hemes is that the oxygen molecule assumes more than one orientation. This disordering of the distal oxygen atom could have made it "invisible" in the electron density map. The 30% occupancy of the proximal oxygen atom site, inferred from the comment on oxidation by Perutz et al. (1987) quoted above, is consistent with this hypothesis. Thus the ratio of occupancies of the α and β hemes in the electron density map may in fact be consistent with the optical results.

The Amount of Cooperativity Observed in the Crystal Suggests Only a Slight Perturbation on an Allosteric Model. Shulman et al. (1975, 1982) emphasized that the independence of the affinity on the number of ligands bound to a single quaternary structure is the essential element of the MWC two-state allosteric model. Up to now it has not been possible to rigorously test this all-important prediction, because no experiment has been performed on unmodified hemoglobin in which the quaternary structure was known to remain unchanged throughout the binding curve. The apparent crystal binding curves are almost perfectly noncooperative (Figure 9). However, one of the more interesting and subtle aspects of ligand binding is that cooperativity within the tetramer can be masked by inequivalence in the affinity of the α and β subunits. Because we obtained the α and β subunit binding curves separately (Figure 15), we can evaluate the magnitude of this cooperativity.

The simplest scheme for introducing cooperativity into oxygen binding by the T quaternary structure is to assume that the dimer is the cooperative unit, as was done by Brunori and co-workers in formulating the "cooperon" model (Brunori et al., 1986; Gill et al., 1986). The binding polynomial for

[4] Waller and Liddington (1990) found that IHP is disordered in the crystal and only a single phosphate group is clearly visible. They also found that there are significant differences between the IHP-containing structure and the structure of "semioxyhemoglobin" at IHP binding sites in the β subunits, suggesting that neither IHP nor DPG were present, but undetected, in the latter crystals.

such a tetramer is (Hess & Szabo, 1979; Gill et al., 1986)[5]

$$Q = [1 + (K_\alpha + K_\beta)p + \delta K_\alpha K_\beta p^2]^2 \quad (20)$$

where K_α and K_β are the binding constants for the α and β subunits and δ is the interaction parameter that produces cooperativity. The binding curves, calculated from d ln Q/d ln p, for the α subunits and β subunits are then

$$y_\alpha = \frac{K_\alpha p + \delta K_\alpha K_\beta p^2}{1 + (K_\alpha + K_\beta)p + \delta K_\alpha K_\beta p^2} \quad (21)$$

$$y_\beta = \frac{K_\beta p + \delta K_\alpha K_\beta p^2}{1 + (K_\alpha + K_\beta)p + \delta K_\alpha K_\beta p^2}$$

and for the tetramer

$$y = \frac{1}{2}\frac{(K_\alpha + K_\beta)p + 2\delta K_\alpha K_\beta p^2}{1 + (K_\alpha + K_\beta)p + \delta K_\alpha K_\beta p^2} \quad (22)$$

The detailed shapes of these binding curves are determined by the relative binding constants of the α and β subunits and the magnitude of the interaction parameter, δ. The slope of the Hill plot at the $p50$ for the tetramer binding curve is (Szabo & Karplus, 1975)

$$n = \frac{4}{2 + (q + 1)/(\delta q)^{1/2}} \qquad q \equiv K_\alpha/K_\beta \quad (23)$$

This relation shows that there is a continuous range of values for the ratio of α and β affinities and the interaction parameter δ that produce a particular Hill n for the tetramer binding curve. Moreover, any combination of q and δ which yields $n = 1$ [for which eq 23 becomes $\delta = (q + 1)^2/4q$] produces a linear Hill plot with a unit slope at all pressures. That is, within this model cooperativity of any magnitude will be completely masked by inequivalent binding to the α and β subunits to produce a noncooperative binding curve for the tetramer. Therefore, the unique determination of the subunit affinities and the interaction parameter requires analysis of the individual binding curves for the α and β subunits.

Figure 15 shows the separate α and β binding curves and the simultaneous fit to these curves using eq 21. The ratio of the intrinsic affinities ($q = K_\alpha/K_\beta$) is 4.6 ± 0.4, and the interaction parameter is 1.8 ± 0.3. The uncertainties represent the standard deviation from the mean of the three determinations in Figure 15. The real uncertainties are larger than this, because the quantities q and δ are sensitive to the heme orientations. The heme orientations are known from X-ray crystallography for the deoxygenated α and β subunits, as well as for the oxygenated α subunit, but are not known with certainty for the oxygenated β subunit (Table I).

In the absence of any cooperativity, the ratio of affinities of 4 would yield a Hill n over the range of pressures of our experiments of 0.89 for the tetramer. The finding of a slope of 1.0 for the tetramer (Figure 15) results from the compensation of the inequivalence in the α and β subunit affinities and the small amount of cooperativity. It is interesting in this regard that small conformational changes of the β subunit upon carbon monoxide binding to the α-subunit have been observed in the metal hybrid $\alpha(FeCO)_2\beta(Ni)_2$ (Luisi & Shibayama, 1989).

The value of 1.8 for the interaction parameter should be compared with the difference in the affinities for the T- and R-states in solution, which is about a factor of 300 at neutral pH (Imai, 1982). In terms of free energy, the cooperativity within the T quaternary structure in the crystal is only about 10% of the cooperativity generated by the change in quaternary structure from T to R. It appears, then, that the cooperativity within the T quaternary structure represents only a slight perturbation on the most essential idea of the MWC two-state allosteric model.

One can of course argue that our results do not disprove sequential models of the Pauling type (Pauling, 1935; Koshland et al., 1966).[6] One would simply postulate that the crystal lattice forces prevent the tertiary conformational changes that occur in solution and that are responsible for cooperative binding. More specifically, the tertiary conformational change that ruptures the salt bridges to produce the tertiary Bohr effects (Figures 1 and 17) could also lead to cooperative interaction. There is evidence from studies by Shibayama et al. (1986) on nickel hybrids to counter this argument. In these molecules the iron in either the α or β hemes has been substituted by nickel(II). The nickel porphyrins do not bind oxygen. At neutral pH it is assumed that these molecules remain in the T quaternary structure after binding two oxygen molecules, because the affinity is very similar to that of normal hemoglobin for binding the first oxygen molecule. In both α- and β-substituted molecules the Hill n at neutral pH is 1.0, indicating that there is no cooperative interaction between α subunits and none between β subunits.[7] There is, however, a pH dependence to the affinity, demonstrating that it is possible to have noncooperative binding with a Bohr effect.

There are as yet no oxygen binding curves in solution to indicate the extent of intersubunit interaction, if any, between α and β subunits. However, Ackers et al. (1992) have suggested that binding to the T quaternary structure in solution is complex, with both positive and negative cooperativity. This conclusion is based on an analysis of tetramer–dimer dissociation equilibria in metal-substituted and cyanomethemoglobin hybrid molecules. Of the 10 ligation states, only one exhibits a dissociation constant that leads to a major inconsistency with the predictions of the two-state allosteric model (Ferrone, 1986; Gill et al., 1986). This doubly-liganded species, with ligands bound to an α and β subunit in the configuration $\alpha 1(x)\beta 1(x)\alpha 2\beta 2$, is presumed to be in the T quaternary structure. The fact that it behaves differently from the doubly-liganded species with the alternate configuration $[\alpha 1(x)\beta 1\alpha 2\beta 2(x)]$ is inconsistent with a two-state model. From the thermodynamic linkage between oxygen

[5] The binding polynomial for the tetramer for a model with both cooperativity and α,β inequivalence in the T-state, but noncooperativity and equivalent subunits in the R-state, is (Gill et al., 1986) $Q = [1 + 2K_R p + \delta K_R^2 p^2]^2 + L[1 + (K_{T\alpha} + K_{T\beta})p + \delta K_{T\alpha}K_{T\beta}p^2]^2$, where L is the equilibrium constant (≡[T]/[R]) for the unliganded R- and T-states, K_R is the binding constant for all subunits in the R-state, $K_{T\alpha}$ and $K_{T\beta}$ are the T-state binding constants, and δ is the interaction parameter that produces cooperativity in the T-state.

[6] It is often not appreciated that a sequential model cannot explain the important kinetic observation that the rate of carbon monoxide binding depends on the quaternary conformation and not on the number of ligands bound (Hopfield et al., 1971; Cassoly et al., 1971; Sawicki & Gibson, 1976; Shulman et al., 1982; Jones et al., 1992). A sequential model would have to postulate that these species are kinetic transients and are therefore irrelevant because they do not correspond to equilibrium species.

[7] For the $\alpha(Ni)_2\beta(Fe)_2$ hybrid the Hill n was found to be 1.0 at pH's 6.5, 7.5, and 8.5 in 50 mM bis-Tris or Tris buffer plus 0.1 M chloride (Shibayama et al., 1986). The corresponding values for the $\alpha(Fe)_2\beta(Ni)_2$ hybrid were 1.0, 1.1, and 1.3. Since the relative stability of the T quaternary structure decreases with increasing pH (Imai, 1982), it is unlikely that the values greater than 1.0 reflect a change in quaternary structure rather than cooperative interaction between the α subunits at the higher pH's.

binding and subunit dissociation, the anomalous behavior of this species requires that there is cooperativity in its formation.

The amount of cooperativity within the T quaternary structure upon binding the first two ligands to form $\alpha 1(x)$-$\beta 1(x)\alpha 2\beta 2$ depends on the system (Ackers et al., 1992). In the cyanometHb system, in which metheme with cyanide bound is taken as a model for an oxygenated heme, the second ligand binds with an affinity that is increased by a factor of 170 compared to the first ligand, an affinity difference that is comparable to what is believed to be the difference between R and T in a two-state analysis of oxygen binding curves. In the cobalt hybrid system the heme–carbon monoxide complex is taken as a model for an oxygenated heme and unliganded cobalt-substituted heme for the deoxyheme. In this system the factor is only 2.5, close to our value of 1.8 for δ, and should therefore be regarded as only a perturbation on a two-state allosteric model. Furthermore, Perella et al. (1990) have determined the fraction of intermediate species by low-temperature isoelectric focusing of hemoglobin partially saturated with carbon monoxide and found concentrations that yield a value of δ of 2.7 (+3.6, −1.5).

SUMMARY AND CONCLUSIONS

Although hemoglobin crystals from a variety of species have been available since 1871 (Preyer, 1871; Reichert & Brown, 1909), and accurate oxygen binding curves on hemoglobin solutions have been measured since 1904 (Bohr et al., 1904), the present work represents the first measurement of an oxygen binding curve for crystals of hemoglobin. We have shown that by measuring spectra over a wide wavelength range, it is possible to obtain very precise and reproducible binding curves in spite of significant oxidation to metHb. The behavior of hemoglobin in the crystal is very different from that of hemoglobin in solution, presumably because of the prevention of protein conformational changes by the lattice forces. With the development of this technique it is now possible to carry out structure–function studies of hemoglobin without the ambiguities of differences in structure between hemoglobin in the crystal and in solution.

Our data clearly show that binding of oxygen to hemoglobin in the T quaternary structure is essentially noncooperative, confirming the most critical element of the two-state allosteric model for cooperativity of Monod, Wyman, and Changeux. A small amount of cooperativity is exactly compensated by inequivalence in the affinities of the α and β subunits to produce a binding curve for the tetramer with a Hill n of 1.0. Unlike the T quaternary structure in solution, the crystal binding curves exhibit no Bohr effect. Since the salt bridges remain intact upon oxygen binding, this is a necessary result for the validity of the Perutz stereochemical mechanism for the Bohr effect in which the salt bridges play the central role (Perutz, 1970). It is perhaps ironic that the oxygen binding properties of hemoglobin in the *crystal* are so different from those of hemoglobin in *solution*, yet they support Perutz's stereochemical mechanism for cooperativity in *solution*, which was based on the structure of hemoglobin in the *crystal*.

The absence of the Bohr effect and the low affinity of the crystal suggest a generalization of the MWC–PSK model in which both high- and low-affinity conformations, with broken and unbroken salt bridges, respectively, are populated in the T quaternary structure. This model makes interesting and readily testable predictions on the relation between the tertiary Bohr effect and the affinity of the T quaternary structure.

A unique aspect of the crystal experiments is that it is possible to obtain the relative affinities of the α and β hemes. We find that the α hemes have about a 5-fold higher affinity than the β hemes. This is quite different from the interpretation of the electron density map of the partially oxygenated crystal (Brzozowski et al., 1984a; Liddington et al., 1988). We suggest that the extent of binding to the α hemes in the X-ray study was overestimated because of interference from the oxygen atoms of water molecules present in both metHb and deoxyHb. We also suggest that the extent of oxygen binding to the β hemes was underestimated because of multiple orientations of the oxygen molecule. Clearly, what is needed at this point is an investigation in which X-ray data collection is carried out on crystals that are simultaneously monitored by optical spectroscopy to determine the composition in terms of oxy-, deoxy-, and methemes.

Another novel aspect of this work was the discovery of the kinetics of conformational changes in the crystal. The kinetics are so slow compared to oxygen binding and dissociation that they can be monitored by the oxygen affinity. These observations open up a completely new area of investigation on the kinetics of protein conformational changes. We assume that the kinetics correspond to those of the change in quaternary structure, but this has yet to be proven. Perhaps time-resolved X-ray crystallography in combination with an optical study can provide the answer.

ACKNOWLEDGMENT

We thank Attila Szabo for many helpful discussions, Eduardo Padlan for X-ray diffraction measurements, and Robert Liddington and Ben Luisi for providing us with unpublished coordinates.

REFERENCES

Abraham, D. J., Peascoe, R. A., Randad, R. S., & Panikker, J. (1992) *J. Mol. Biol. 227*, 480–492.
Ackers, G., Doyle, M. L., Myers, D., & Daugherty, M. A. (1992) *Science 255*, 54–63.
Amiconi, G., Bonaventura, C., Bonaventura, J., & Antonini, A. (1977) *Biochim. Biophys. Acta 495*, 279–286.
Anderson, L. (1973) *J. Mol. Biol. 79*, 495–506.
Anderson, L. (1975) *J. Mol. Biol. 94*, 33–49.
Antonini, E., Wyman, J., Brunori, M., Fronticelli, C., Bucci, E., & Rossi-Fanelli, A. (1965) *J. Biol. Chem. 240*, 1096–1103.
Arnone, A., Rogers, P., Blough, N., McGourty, J., & Hoffman, B. (1986) *J. Mol. Biol. 188*, 693–706.
Baldwin, J., & Chothia, C. (1979) *J. Mol. Biol. 129*, 175–220.
Bohr, C., Hasselbach, K. A., & Krogh, A. (1904) *Skand. Arch. Physiol. 16*, 401–412.
Brunori, M., Coletta, M., & Di Cera, E. (1986) *Biophys. Chem. 23*, 215–222.
Brzozowski, A., Derewenda, Z., Dodson, E., Dodson, G., Grabowski, M., Liddington, R., Skarzynski, T., & Vallely, D. (1984a) *Nature 307*, 74–76.
Brzozowski, A., Derewenda, Z., Dodson, E., Dodson, G., Liddington, R., Skarzynski, T., & Vallely, D. (1984b) in *Hemoglobin: Structure and Function* (Schnek, A. G., & Paul, C., Eds.) pp 36–50, Edition de l'Universite de Bruxelles.
Cassoly, R., Gibson, Q. H., Ogawa, S., & Shulman, R. G. (1971) *Biochem. Biophys. Res. Commun. 44*, 1015–1021.
Chu, A. H., Turner, B. W., & Ackers, G. K. (1984) *Biochemistry 23*, 604–617.
Daugherty, M. A., Shea, M. A., Johnson, J. A., LiCata, V. J., Turner, G. J., & Ackers, G. K. (1991) *Proc. Natl. Acad. Sci. U.S.A. 88*, 1110–1114.
Dickerson, R. E., & Geis, I. (1983) *Hemoglobin*, Benjamin/Cummings, London.
Dozy, A. M., Kleihauer, E. F., & Huisman, T. H. J. (1968) *J. Chromatogr. 32*, 723–727.

Dvorak, J. A., & Stotler, W. F. (1971) *Exp. Cell Res. 68*, 144–148.
Eaton, W. A., & Hochstrasser, R. M. (1967) *J. Chem. Phys. 46*, 2533–2539.
Eaton, W. A., & Hochstrasser, R. M. (1968) *J. Chem. Phys. 49*, 985–995.
Eaton, W. A., & Hofrichter, J. (1981) *Methods Enzymol. 76*, 175–261.
Edelstein, S. J. (1975) *Annu. Rev. Biochem. 44*, 209–232.
Fermi, G., & Perutz, M. F. (1981) in *Atlas of Molecular Structures in Biology. 2. Haemoglobin and Myoglobin* (Phillips, D. C., & Richards, F. M., Eds.) Clarendon Press, Oxford, England.
Ferrone, F. A. (1986) *Proc. Natl. Acad. Sci. U.S.A. 83*, 6412–6414.
Gill, S. J. (1981) *Methods Enzymol. 76*, 427–438.
Gill, S. J., Robert, C. H., Coletta, M., Di Cera, E., & Brunori, M. (1986) *Biophys. J. 50*, 747–752.
Grabowski, M. J., Brzozowski, A. M., Derewenda, Z. S., Skarzynski, T., Cygler, M., Stepien, A., & Derewenda, A. E. (1978) *Biochem. J. 171*, 277–279.
Haire, R. N., Tisel, W. A., Niazi, G., & Rosenberg, A. (1981) *Biochem. Biophys. Res. Commun. 101*, 177–182.
Haurowitz, F. (1938) *Z. Physiol. Chem. 234*, 266.
Herzfeld, J., & Stanley, H. E. (1974) *J. Mol. Biol. 82*, 231–265.
Hess, V. L., & Szabo, A. (1979) *J. Chem. Educ. 56*, 289–293.
Hofrichter, J., & Eaton, W. A. (1976) *Annu. Rev. Biophys. Bioeng. 5*, 511–560.
Hopfield, J. J., Schulman, R. G., & Ogawa, S. (1971) *J. Mol. Biol. 61*, 425–443.
Imai, K. (1979) *J. Mol. Biol. 133*, 233–247.
Imai, K. (1982) *Allosteric Effects in Hemoglobin*, Cambridge University Press, Cambridge, England.
Janin, J., & Wodak, S. (1985) *Biopolymers 24*, 509–526.
Johnson, M. L., Turner, B. W., & Ackers, G. K. (1984) *Proc. Natl. Acad. Sci. U.S.A. 81*, 1093–1097.
Jones, C. M., Ansari, A., Henry, E. R., Hofrichter, J., & Eaton, W. A. (1991) *Biochemistry 31*, 6692–6702.
Koshland, D. E., Nemethy, G., & Filmer, D. (1966) *Biochemistry 5*, 365–385.
Lalezari, I., Lalezari, P., Poyart, C., Marden, M., Kister, J., Bohn, B., Fermi, G., & Perutz, M. F. (1990) *Biochemistry 29*, 1515–1523.
Lee, A., & Karplus, M. (1983) *Proc. Natl. Acad. Sci. U.S.A. 80*, 7705–7059.
Lee, A., Karplus, M., Poyart, C., & Bursaux, E. (1988) *Biochemistry 27*, 1285–1301.
Lesk, A. M., Janin, J., Wodak, S., & Chothia, C. (1985) *J. Mol. Biol. 183*, 267–270.
Liddington, R. C. (1986) D.Phil. Thesis, University of York, England.
Liddington, R., Derewenda, Z., Dodson, G., & Harris, D. (1988) *Nature 331*, 725–728.
Luisi, B., & Shibayama, N. (1989) *J. Mol. Biol. 206*, 723–736.
Luisi, B., Liddington, B., Fermi, G., & Shibayama, N. (1990) *J. Mol. Biol. 214*, 7–14.
Makinen, M. W., & Eaton, W. A. (1974) *Nature 247*, 62–64.
Makinen, M. W., & Churg, A. K. (1983) in *Iron Porphyrins, Part I* (Lever, A. B. P., & Gray, H. B., Eds.) pp 141–235, Addison-Wesley, London.
Marden, M. C., Bohn, B., Kister, J., & Poyart, C. (1990) *Biophys. J. 57*, 397–403.
McPherson, A. (1976) *J. Biol. Chem. 251*, 6300–6303.
McPherson, A. (1985) *Methods Enzymol. 114*, 120–125.
McPherson, A. (1990) *Eur. J. Biochem. 189*, 1–23.
Mills, F. C., Johnson, M. L., & Ackers, G. K. (1976) *Biochemistry 15*, 5351–5362.
Monod, J., Wyman, J., & Changeux, J.-P. (1965) *J. Mol. Biol. 12*, 88–118.
Mozzarelli, A., Peracchi, A., Rossi, G. L., Ahmed, S. A., & Miles, E. W. (1989) *J. Biol. Chem. 264*, 15774–15780 (and references therein).
Mozzarelli, A., Rivetti, C., Rossi, G. L., Henry, E. R., & Eaton, W. A. (1991) *Nature 351*, 416–419.
Ownby, D. W., & Gill, S. J. (1990) *Biophys. Chem. 37*, 395–406.
Pauling, L. (1935) *Proc. Natl. Acad. Sci. U.S.A. 21*, 186.
Perrella, M., Colosimo, A., Benazzi, L., Ripamonti, M., & Rossi-Bernardi, L. (1990) *Biophys. Chem. 37*, 211–223.
Perutz, M. F. (1953) *Acta Crsytallogr. 6*, 859–864.
Perutz, M. F. (1970) *Nature 228*, 726–739.
Perutz, M. F. (1976) *Br. Med. Bull. 32*, 195–208.
Perutz, M. F. (1989) *Q. Rev. Biophys. 22*, 139–287.
Perutz, M. F., Bolton, W., Diamond, R., Muirhead, H., & Watson, H. C. (1964) *Nature 203*, 687–690.
Perutz, M. F., Fersht, A. R., Simon, S. R., & Roberts, G. C. K. (1974) *Biochemistry 13*, 2174–2186.
Perutz, M. F., Kilmartin, J. V., Nagai, K., Szabo, A., & Simon, S. R. (1976) *Biochemistry 15*, 378–387.
Perutz, M. F., Fermi, G., Luisi, B., Shaanan, B., & Liddington, R. C. (1987) *Acc. Chem. Res. 20*, 309–321.
Preyer, W. (1871) *Die Blutkrystalle*, Mauke's Verlag, Jena.
Ray, W. J., & Puvathingal, J. M. (1985) *Anal. Biochem. 146*, 307–312.
Ray, W. J., Bolin, J. T., Puvathingal, J. M., Minor, W., Liu, Y., & Muchmore, S. W. (1992) *Biochemistry 30*, 6866–6875.
Reichert, E. T., & Brown, A. P. (1909) *The Differentiation and Specificity of Corresponding Proteins and Other Vital Substances in Relation to Biological Classification and Organic Evolution: The Crystallography of Hemoglobins*, Carnegie Institution, Washington, DC.
Rossi, G. L., & Bernhard, S. A. (1970) *J. Mol. Biol. 49*, 85–91.
Rossi, G. L., Mozzarelli, A., Peracchi, A., & Rivetti, C. (1992) *Philos. Trans. R. Soc. London A340*, 191–207.
Rossi-Bernardi, L., Perrella, M., Luzzana, M., Samaja, M., & Raffaele, I. (1977) *Clin. Chem. 23*, 1215–1225.
Sawicki, C. A., & Gibson, Q. H. (1976) *J. Biol. Chem. 251*, 1533–1542.
Shaanan, B. (1983) *J. Mol. Biol. 171*, 31–59.
Shibayama, N., Morimoto, H., & Miyazaki, G. (1986) *J. Mol. Biol. 192*, 331–336.
Shulman, R. G., Hopfield, J. J., & Ogawa, S. (1975) *Q. Rev. Biophys. 8*, 325–420.
Shulman, R. G., Ogawa, S., & Mayer, A. (1982) in *Hemoglobin and Oxygen Binding* (Ho, C., et al., Eds.) pp 206–209, Elsevier Biomedical, New York.
Szabo, A., & Karplus, M. (1972) *J. Mol. Biol. 72*, 163–197.
Szabo, A., & Karplus, M. (1975) *Biochemistry 14*, 931–940.
Tan, A. L., & Noble, R. W. (1973) *J. Biol. Chem. 248*, 7412–7416.
Waller, D. A., & Liddington, R. C. (1990) *Acta Crystallogr. B46*, 409–418.
Ward, L. B., Wishner, B. C., Lattmann, E. E., & Love, N. E. (1975) *J. Mol. Biol. 98*, 161–177.
Williams, R. C., & Tsay, K.-Y. (1973) *Anal. Biochem. 54*, 137–145.